Atmospheric
Chemistry
and Physics
Discussions

Open Access

OClO and BrO observations in the volcanic plume of Mt. Etna – implications on the chemistry of chlorine and bromine species in volcanic plumes

J. Gliß[1,2], N. Bobrowski[1], L. Vogel[3], and U. Platt[1]

[1]Institute for Environmental Physics, Heidelberg, Germany
[2]Norwegian Institute for Air Research (NILU), Kjeller, Norway
[3]Earth Observation Science, Space Research Centre, Department of Physics and Astronomy, University of Leicester, UK

Correspondence to: Jonas Gliß (jonas.gliss@nilu.no)

Discussion Paper | Discussion Paper | Discussion Paper | Discussion Paper

ACPD

14, 25213–25280, 2014

OClO and BrO observations in the volcanic plume of Mt. Etna

Gliß et al.

Title Page

Abstract | Introduction

Conclusions | References

Tables | Figures

◄◄ | ►►

◄ | ►

Back | Close

Full Screen / Esc

Printer-friendly Version

Interactive Discussion

Abstract

Spatial and temporal profiles of chlorine dioxide (OClO), bromine monoxide (BrO) and sulphur dioxide (SO_2) were measured in the plume of Mt. Etna, Italy, in September 2012 using Multi-Axis-Differential-Optical-Absorption-Spectroscopy (MAX-DOAS).

OClO (BrO) was detected in 119 (452) individual measurements covering plume ages up to 6 (23) minutes. The retrieved slant column densities (SCDs) reached values up to 2.0×10^{14} molecules cm^{-2} (OClO) and 1.1×10^{15} molecules cm^{-2} (BrO). In addition, the spectra were analysed for signatures of IO, OIO and OBrO, none of these species could be detected. The corresponding detection limits for IO/SO_2, OIO/SO_2 and $OBrO/SO_2$ were 1.8×10^{-6}, 2.0×10^{-5} and 1.1×10^{-5} respectively.

The measurements were performed at plume ages (τ) from zero to 23 min downwind the emission source. The chemical variability of BrO and OClO in the plume was studied analysing the $OClO/SO_2$ and BrO/SO_2-ratio. A marked increase of both ratios was observed in the young plume ($\tau < 3$ min) and a levelling off at larger plume ages ($\tau > 3$ min) with mean abundances of 3.17×10^{-5} ($OClO/SO_2$), 1.55×10^{-4} (BrO/SO_2) and 0.16 ($OClO/BrO$). Furthermore, enhanced BrO/SO_2-ratios were found at the plume edges (by $\sim$ 30–37 %) and a strong indication of enhanced $OClO/SO_2$-ratios as well ($\sim$ 10–250 %). A measurement performed in the early morning (05:20–06:20 UTC, sunrise: 04:40 UTC) showed an BrO/SO_2-ratio increasing with time until 05:35 UTC and a constant ratio afterwards. Observing this increase was only possible due to a correction for stratospheric BrO signals in the plume spectra. The corresponding $OClO/SO_2$-ratio showed a similar trend stabilising around 06:13 UTC, approximately 40 min later than BrO. This is another strong indication for the photochemical nature of the reactions involved in the formation of oxidised halogens in volcanic plumes. In particular, these findings support the current understanding of the underlying chemistry, namely, that BrO is formed in an autocatalytic reaction mechanism in literature often referred to as "bromine explosion" and that OClO is formed in the "BrO + ClO"-reaction.

BrO and OClO concentrations were estimated from the measured SCDs assuming a circular plume shape. In addition, mixing ratios of ClO were determined from the retrieved OClO and BrO-SCDs assuming chemical equilibrium between formation of OClO (BrO + ClO) and its destruction (photolysis). Mean abundances in the young plume ($\tau < 4\,\text{min}$) were $\overline{\text{BrO}} = 1.35\,\text{ppb}$, $\overline{\text{OClO}} = 300\,\text{ppt}$ and $\overline{\text{ClO}} = 139\,\text{ppt}$ with peak values of 600 ppt (OClO), 2.7 ppb (BrO) and 235 ppt (ClO) respectively.

The prevailing Cl-atom concentrations in the plume could be estimated from the rate of increase of OClO and BrO in the young plume and the determined ClO and OClO concentrations. Values between $5.1 \times 10^6\,\text{cm}^{-3}$ (at 40 ppb O_3) and $2.1 \times 10^8\,\text{cm}^{-3}$ (at 1 ppb O_3) were found. Based on that, a potential – chlorine induced – depletion of tropospheric methane (CH_4) in the plume was investigated. CH_4-lifetimes between 13 h (at 1 ppb O_3) and 23 days (at 40 ppb O_3) were found. These are considerably small compared to the atmospheric lifetime of CH_4. However, the impact of gaseous chlorine on the CH_4-budget in the plume environment was assessed to be relatively small, mainly due to plume dispersion (decrease of Cl number densities) and permanent mixing of the plume with the surrounding atmosphere (net supply of O_3 and CH_4).

1 Introduction

In the past years, improved measurement techniques, especially remote sensing methods, gained importance for the study of the chemical composition of volcanic plumes. Here we present MAX-DOAS measurements (e.g. Hönninger et al., 2004) of the halogen-oxides BrO and OClO in the volcanic plume of Mt. Etna on Sicily, Italy. MAX-DOAS is an established method to study the chemical composition of volcanic plumes by analysing scattered sunlight spectra. It is therefore possible to analyse a large variety of different plume ages without being exposed to the dangers and difficulties often associated with in-situ gas measurements. A detailed understanding of volcanic emissions and the chemistry involved can be helpful for approaches related to volcanic risk assessment and the prediction of volcanic eruptions (see e.g. Carroll and Holloway,

1994; Donovan et al., 2014). Furthermore, volcanic emissions can have significant impacts on the atmosphere and the climate both on regional and global scales (e.g. Robock, 2000). A detailed knowledge of the chemical composition of volcanic plumes and the evolution of – potentially climate-relevant – chemical species is therefore help-
5 ful to better assess potential impacts and influences on climate and atmosphere.

The focus of this article is on the chemistry of halogens in volcanic plumes, especially the formation of reactive halogen species (RHS, e.g. BrO, ClO, OClO) from the primarily emitted species (e.g. HCl, HBr) and their evolution in the ageing plume. The interest in studying RHS in volcanic plumes increased drastically in 2003, when large
10 amounts of bromine monoxide (BrO) were detected in the plume of Soufriére Hills volcano, Montserrat (Bobrowski et al., 2003). Today, we have only gained a rough understanding of the chemical processes involved in the RHS-formation in volcanic plumes and possible dependencies due to the presence of other species (e.g. ozone or oxides of nitrogen). Especially the conversion of the emitted HCl into oxidised chlorine com-
15 pounds (ClO, OClO) in the plume is still poorly understood. This is both due to a lack of measurement data and the complexity of the chemical processes involved.

1.1 Halogens in volcanic plumes

According to current knowledge, volcanic halogens are mainly emitted in the rather un-reactive form of hydrogen halides such as HCl, HF, HBr, HI (e.g. Carroll and Hol-
20 loway, 1994; Francis et al., 1995; Gerlach, 2004). Pyle and Mather (2009) reviewed past measurements ($\sim$ 1980–2008) of arc-related volcanic halogen emissions around the globe and provided estimations of global fluxes of these species. According to their findings, HCl contributes most with an estimated flux of $4.3\,(\pm 1)\,\mathrm{Tg\,a^{-1}}$ whereas HBr and HI emissions are orders of magnitude smaller with fluxes of $5\text{–}15\,\mathrm{Gg\,a^{-1}}$ and 0.5–
25 $2\,\mathrm{Gg\,a^{-1}}$ respectively.
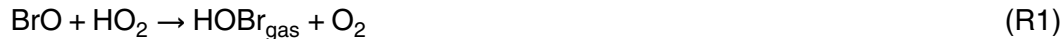
1.1.1 Volcanic bromine

Several model studies indicate, that a certain amount of RHS (e.g. Cl, Br) can be produced in the hot initial plume via high temperature oxidative dissociation processes (Gerlach, 2004; Martin et al., 2006). Br can also be formed via reaction of HBr with OH in the very young plume (Roberts et al., 2009). However, in case of the BrO formation, photochemical reactions have to be additionally involved once the gases are exposed to the atmosphere (e.g. Bobrowski et al., 2007; Oppenheimer et al., 2006). This could be confirmed by direct observations showing an increase of the BrO/SO_2-ratio in the young plume (with increasing plume age) and a levelling off afterwards (e.g. Bobrowski et al., 2007; Bobrowski and Giuffrida, 2012)[1]. This is a further strong indication that the largest part of the observed BrO is formed within the plume, rather than directly emitted by the volcano itself or entirely formed in high temperature reactions directly after emission.

The formation of gaseous BrO in the plume is most likely driven by a heterogeneous and partly auto-catalytic reaction mechanism often referred to as "bromine explosion" (e.g. Lehrer et al., 1997; Wennberg, 1999). The bromine explosion encompasses the uptake of hypobromous acid (HOBr) from the gas into the aqueous phase. After reaction of HOBr with bromide, Br_2 is released to the gas phase. The mechanism is mainly described by the following Reactions (R1)–(R5):

$$BrO + HO_2 \rightarrow HOBr_{gas} + O_2 \tag{R1}$$

$$HOBr_{gas} \rightarrow HOBr_{aq} \tag{R2}$$

$$HBr_{gas} \rightarrow HBr_{aq} \rightarrow Br^-_{aq} + H^+_{aq} \tag{R3}$$

$$HOBr_{aq} + Br^-_{aq} + H^+_{aq} \rightarrow Br_{2,\,gas} + H_2O \tag{R4}$$

---

[1]Note: SO_2 is treated as a passive plume tracer, the ratio is used to cancel out plume dispersion effects in the measured SCDs (for details see Sect. 2.9).

The subscript "aq" denotes species in the aquatic phase on particles. BrO is then formed by the reaction of O_3 with Br radicals which are produced by the photolysis of Br_2:

$$2Br + 2O_3 \rightarrow 2BrO + 2O_2 \tag{R5}$$

5   Once formed, the self reaction of BrO induces a catalytic destruction of O_3.

1.1.2   Volcanic chlorine

Possible formation-processes of reactive chlorine from the emitted HCl (see Sect. 1.1) are still little studied. A chlorine-equivalent to the "bromine explosion" is unlikely (e.g. von Glasow et al., 2009). Most of the emitted HCl rather stays un-reactive in the
10 gaseous phase. Only a part of the HCl is dissolved in the aerosol or cloud droplets. The chloride ions are, however, less reactive compared to bromide ions (see R4f) (von Glasow et al., 2009). Rather, Cl-release is likely to be a by-product of the bromine explosion via formation of BrCl in the reaction of HOBr with chloride. According to Fickert et al. (1999) the effectiveness of this – Cl releasing – reaction channel strongly depends
15 on the Cl^-/Br^--ratio in the liquid phase. Only for Cl^-/Br^--ratios of the order of 10^4 a significant release of BrCl was found (e.g. 50 % BrCl and 50 % Br_2 for $Cl^-/Br = 2 \times 10^4$). For Cl^-/Br^--ratios below 10^3 the HOBr uptake rather yields a release of more than 90 % Br_2. Direct sampling measurements at Mt. Etna revealed Cl^-/Br^--ratios of the order of 10^2 (Martin et al., 2008) to 10^3 (Wittmer et al., 2014). To our knowledge, there
20 are no measurements indicating Cl^-/Br^--ratios of the order of 10^4 at Mt. Etna. We therefore assess the BrCl release to be relatively small in the case of Mt. Etna.

Measurements of reactive chlorine compounds in volcanic plumes are rare. The underlying chemistry is therefore only partly understood and still bears large uncertainties, especially in terms of possible abundances of Cl-atoms in the gaseous phase.
25 Once these are provided, the follow-up reactions producing ClO and OClO are more

straight forward: in analogy to BrO, ClO is likely formed via reaction with O_3 and OClO is then formed via the following reaction:

$$BrO + ClO \rightarrow OClO + Br \tag{R6}$$

The corresponding reaction rate coefficient is $k_1 = 6 \times 10^{-12}\,cm^3\,s^{-1}$ (at 298 K, Sander et al., 2006). Further possible reactions for the formation of OClO are orders of magnitude slower (e.g. $ClO + O_3$, $ClO + ClO$, Sander et al., 2006) and were not considered within this study. The main daytime sink of OClO is its photolysis:

$$OClO + h\nu \xrightarrow{J} ClO + O \quad J \approx 6 \times 10^{-2}\,s^{-1}. \tag{R7}$$

Both Bobrowski et al. (2007) and General et al. (2014) detected OClO in the plume of Mt. Etna. The corresponding OClO/SO_2-ratios were between $3\text{–}6 \times 10^{-5}$ (for spectra related to the plume centre). Simultaneous BrO measurements indicate an OClO/BrO-ratio of approximately 0.25 for Mt. Etna in both studies. Further detections of volcanic OClO are reduced to satellite measurements in the plume of Puyehue-Cordón Caulle volcano (Chile) after an eruption in 2011 (Theys et al., 2014) and most recently, the detection of OClO in the plume of Soufriére Hills volcano during a hiatus in 2011 was reported (Donovan et al., 2014). Compared to the measurements at Mt. Etna, the corresponding OClO/SO_2-ratios are high ($4\text{–}6 \times 10^{-4}$) as well as the OClO/BrO-ratios showing values up to 5 (i.e. about 20 times larger than OClO/BrO-ratios at Mt. Etna).

Key parameter for the OClO formation in volcanic plumes is the prevailing availability of ClO and BrO molecules. Previous studies reported relatively high amounts of volcanic ClO measured with passive DOAS instruments (Bobrowski et al., 2007; Lee et al., 2005). The corresponding ClO/SO_2 ratios were of the order of 5 % hence, almost three orders of magnitude more ClO than OClO. However, these measurements have to be treated cautiously due to difficulties and uncertainties in the DOAS evaluation of ClO. These evaluation problems are mainly caused by the very low intensity

of scattered sunlight in the ClO evaluation wavelength range (308 nm and below) and possible interferences with other trace gases such as SO_2 or O_3. Furthermore, to our knowledge it has not yet been possible to reproduce these measurements in model studies (e.g. Bobrowski et al., 2007; von Glasow, 2010). Kern et al. (2009) investigated ClO and OClO abundances at the vent of Masaya Volcano in Nicaragua using an active Long-Path DOAS instrument. They did not detect any of both species. This is probably due to the proximity of the measurement to the crater, where the RHS formation is still in an early stage. Furthermore, the halogen-content of the Masaya volcano plume is probably smaller compared to Mt. Etna (Pyle and Mather, 2009). By assuming equilibrium between formation (R6) and destruction (R7) of OClO, Kern et al. (2009) found that ClO and OClO abundances in volcanic plumes should be of the same order of magnitude during daytime. This is in good agreement with the findings of General et al. (2014) who did the same calculation for the Etna data using their BrO and OClO retrieval. However, according to Theys et al. (2014) this seems not to be the case for the plume of the Puyehue–Cordón Caulle eruption in 2011 which rather indicates a large excess of ClO compared to BrO and OClO.

The focus of this study is on MAX-DOAS measurements performed in the plume of Mt. Etna (Sicily) in September 2012. We were able to directly observe the formation of BrO and OClO in the young plume. In addition, we found evidences of the photochemical nature of the reactions involved. ClO and Cl concentrations in the plume were estimated and based on that, a possible (Cl-induced) depletion of tropospheric methane (CH_4) in the plume environment. Possible abundances of other oxidised halogen species (i.e. OBrO, IO, OIO) were investigated but none of those could be detected. In the following section, details on the data acquisition and evaluation are presented. Our results are presented and discussed in Sect. 3.

2 Methods and study area

2.1 Technical setup

The MAX-DOAS instrument used in this study is suited to analyse the solar spectrum both in the ultraviolet (UV) and the visible (VIS) range due to two included spectrographs (Avantes AvaBench-75-Ultra Low Straylight). The two spectrographs cover a spectral range of 292–578 nm (UV: 292.1–456.1 nm, VIS: 434.7–577.8 nm) and are characterised by a high signal-to-noise ratio (S/N-ratio). Scattered sunlight was collected by a small telescope consisting a of a quartz lens ($f = 100$ mm) which focuses the light onto an optical fibre bundle. The fibre bundle consists of seven individual fibres with each a diameter of $d = 100$ µm. Six of these fibres are coupled into the UV spectrograph, the seventh into the VIS respectively. The UV spectrograph has a measured spectral resolution of $\Delta\lambda_{UV} = 0.51$ nm and a *SCHOTT* BG-3 filter behind the entrance slit to reduce stray light. The spectral resolution of the VIS spectrograph was found to be $\Delta\lambda_{VIS} = 0.39$ nm. The telescope was focused such, that both spectrographs have approximately the same field of view (FOV). The FOV was measured in the laboratory and amounts to 0.15° (UV) and 0.16° (VIS) respectively (full aperture angle). The optical benches of both spectrographs were thermally isolated and temperature stabilized using a Peltier element controlled by a *Supercool* PR-59 temperature controller. During the whole measurement campaign, the spectrographs were temperature stabilised to $T_{meas} = 10$°C. The air tight instrument-box was mounted onto a tripod. Two motors (azimuth and elevation) allowed to point the instruments viewing direction at every position in the sky. An embedded PC was used to control the hardware elements. The data acquisition was done using the software MS-DOAS, which was developed by U. Frieß at the Institute of Environmental Physics in Heidelberg. The geo location at each measurement site was recorded by a GPS-receiver included in the instrument.

Previous MAX-DOAS instruments at volcanic sites usually consisted of a single UV-spectrograph. With these instruments, volcanic plumes can only be anlaysed for UV-sensitive species such as SO_2, BrO or OCIO. With the extended range of the instrument

used in this study, it was possible to additionally evaluate species with absorption-lines in the visible range of the solar spectrum. The oxidised halogen species IO, OIO and OBrO were of particular interest for this study. However, none of these species could be detected significantly. The corresponding detection limits are given in Sect. 3.2.

2.2 Measurement location and data acquisition

Mt. Etna is the largest and most active volcano in Europe and is situated in the eastern part of Sicily, an island south of the Italian mainland. The activity of Mt. Etna shows a distinct variability of both quiescent degassing periods and eruptive periods. During the field trip in September 2012, Etna showed a stable quiescently degassing behaviour from the four active craters – North East (NE), Bocca Nuova (BN), Voragine (VOR) and South East crater (SE) – which are located in the summit region at an altitude of approximately 3300 m a.s.l. The first three days of the campaign (11–13 September 2012) took place at the Etna observatory (Pizzi Deneri) which is located about 2.5 km north-east of the active summit at an altitude of 2800 m. In Fig. 1, all measurement locations of the campaign (11–26 September 2012) are indicated.

2.3 Plume scanning routines

Three different plume scanning routines ("scans") were performed in order to study the chemical variability of the measured species in the volcanic plume (see sketch in Fig. 2). One "scan" typically consists of a set of plume spectra plus a subsequently recorded reference spectrum with the telescope pointing into a volcanic gas free atmosphere (for details see Sect. 2.4). The three measurement routines are presented in the following:

Plume evolution scans

The purpose of this scanning routine is to study the chemical composition in dependence of the plume age. The spectra are therefore recorded at different plume ages along the plume propagation direction (typically in the centre of the plume, see Fig. 2a).

Plume cross section scans

Plume cross section scans are performed perpendicular to the plume propagation axis in order to study differences of the plume composition between the centre and the edges of the plume (Fig. 2b).

Point measurements

A certain number of spectra are taken at a fixed point in the plume without changing the telescopes viewing direction. This measurement type is suitable for the analysis of temporal variations in the plume composition (Fig. 2c).

2.4 Data acquisition and DOAS-evaluation

The spectra were analysed using the software package DOASIS (v. 3.2.4422, Kraus, 2006). Details on the scanning routines can be found in Sect. 2.3. The spectra analysed in DOASIS usually consist of several hundred up to 1500 individual co-added spectra, in order to improve the detection sensitivity. A standard DOAS fit (see Platt and Stutz, 2008) was performed for the UV and VIS spectra in order to retrieve SCDs (S_i) of the chemical species i in the plume (in this study mainly: OClO, BrO, SO_2, IO, OBrO, OIO). A Fraunhofer reference spectrum (FRS, $I_0(\lambda)$) was included into the fitting routines to account for solar absorption lines in the spectra (Fraunhofer lines) and atmospheric background absorption. The FRS were recorded with the telescope pointing in the direction of a volcanic gas free atmosphere and close in time to the corresponding plume spectra (usually subsequently to each scan). The latter

is important to keep potential additional stratospheric signals at a minimum. Stratospheric signals arise with increasing differences of the solar zenith angle (SZA) between plume spectrum and FRS (for details see Sect. 2.8). Each FRS-candidate was pre-evaluated regarding its SO_2-content using a convoluted solar background spectrum

5 as FRS (Chance and Kurucz, 2010). Only FRS-candidates with SO_2-SCDs smaller than $SO_2^{FRS} < 5 \times 10^{16}$ molecules cm^{-2} were assessed to be SO_2-free and thus suited as FRS.

In the following, the implemented steps to retrieve the SCDs from the raw-spectra are described in detail for each species. Prior to the DOAS-evaluation, all FRS- and

10 plume spectra were corrected for electronic offset and dark current. Two Ring spectra $(R, R4)$ were included into the fitting routine to account for inelastic scattering effects (Raman scattering) in the atmosphere (Wagner et al., 2009). The first Ring spectrum (R) was calculated from the respective FRS using the provided function of the evaluation software DOASIS (Kraus, 2006). The second $(R4)$ was determined from R and

15 accounts for the λ^{-4}-dependence of the Rayleigh cross section. The $R4$-spectrum was calculated for each evaluation wavelength range separately using the following equation:

$$R4(j) = R(j) \cdot \left(\frac{\lambda(j)}{\lambda_0} \right)^4 - R(j) \tag{1}$$

Here, j denotes the pixel on the detector, $\lambda(j)$ the appropriate wavelength and λ_0 the

20 central wavelength of the evaluation range. $R(j)$ corresponds to the intensity of the Ring spectrum at position j.

All potential absorbers were included into the fitting routine using high resolution literature cross sections (σ_i, see also Table 2). The σ_i were convolved with the line-spread-function of the respective spectrograph and furthermore corrected for saturation effects

25 and the solar I_0 effect (Platt and Stutz, 2008) using the provided functions of the software package DOASIS. In order to correct for any misalignment of the spectrograph, a slight shift (±0.1 nm) and squeeze (±5 %) were allowed for all species included in

the DOAS fit process (FRS, R, $R4$, σ_i). In order to minimize the degrees of freedom in the fitting-routine, shift and squeeze of all σ_i were linked to the strongest absorber in the respective fit range. Details on the different evaluation ranges can be found in Table 1. In case of the SO_2, BrO and OClO evaluation-routines, shift and squeeze were linked to the SO_2 cross section. In case of the IO, OBrO and OIO fitting routines, shift and squeeze were linked to the NO_2-cross section since SO_2 shows no considerable absorption features in the corresponding wavelength regimes. Shift and squeeze of the two Ring spectra were linked to the corresponding FRS. A 3rd order polynomial was applied to each fitting-routine to remove broad band extinction and to reduce for stray light effects within the spectrograph. We furthermore included an additional (0th-order) polynomial to account for any broadband features in the intensity space (e.g. stray light in the instruments housing, for details see Kraus, 2006).

2.4.1 Error treatment

The statistical treatment of the DOAS fitting procedure and hence the retrieved DOAS-fit error bases on the assumption of independent and uncorrelated intensity measurements at each pixel on the detector. In this case, the underlying measurement uncertainty is dominated by pure photon (shot) noise (Poisson statistics). In case of atmospheric trace gas measurements this is unfortunately not fulfilled mainly due to uncertainties in the absorption spectra of the fitted species or additional absorbers and due to the limited optical resolution of the instrument. These effects often cause distinct structures in the residual of the DOAS-fit. Stutz and Platt (1996) showed that the impact of these structures on the retrieved SCDs is mainly dependent on the width of absorption structures in the reference spectrum. Therefore, the retrieved fit errors do often not represent the true measurement uncertainty which can be up to a factor of six larger than the retrieved fit error (Stutz and Platt, 1996).

To account for this effect we multiplied the retrieved DOAS errors by a factor U following the suggestions of Stutz and Platt (1996): $\sigma_{meas} = U \cdot \sigma_{fit}$. The corresponding

detection limit for the fitted species was defined to be $2 \cdot \sigma_{meas}$, representing a detection certainty of 95 %.

In order to obtain a more accurate estimate of the fit uncertainty σ_{meas}, we applied a simple approach by choosing the correction factor U for each spectrum in dependence of the mean peak-to-peak value ($\overline{\Delta}_{res}$) of the corresponding fit-residual:

(i) $\qquad\qquad \overline{\Delta}_{res} > 1.5 \times 10^{-3} \qquad\qquad \Rightarrow \quad U = 4$

(ii) $\qquad 1.5 \times 10^{-3} \geq \overline{\Delta}_{res} > 1.2 \times 10^{-3} \qquad \Rightarrow \quad U = 3.5$

(iii) $\qquad 1.2 \times 10^{-3} \geq \overline{\Delta}_{res} \qquad\qquad\qquad \Rightarrow \quad U = 3$

According to Stutz and Platt (1996), the underestimation of the true measurement error should be independent of the magnitude of the fit-residual. However, for the instrument used in this study we found, that $\overline{\Delta}_{res}$ is in most cases correlated to distinct structures in the fit-residual. We want to point out, that this approach constitutes only a rough – but easy to implement and still conservative – implementation of the interpretation of the retrieved DOAS fit errors (e.g. Donovan et al. (2014) used a fixed correction factor of $U = 3$ for their OClO and BrO evaluation).

In order to study the chemical variability of the observed oxidised halogen species X_mO_n (here X denotes a halogen atom. e.g. BrO, OClO), we analysed the X_mO_n/SO$_2$-ratios of these species (e.g. BrO/SO$_2$, OClO/SO$_2$, for details see Sect. 2.9). The corresponding errors and detection limits of the X_mO_n/SO$_2$-ratios were calculated from the uncertainties in the retrieved SCDs using gaussian error propagation.

In the following subsections we present the fitting-routines for all species which were evaluated in this work and give the corresponding literature cross sections which were used for the DOAS-fit.

2.4.2 BrO and OClO evaluation routines

BrO and OClO were evaluated in the same wavelength range between 330.6 and 356.3 nm. This range includes the five strongest differential absorption bands of BrO and three of the most pronounced bands of OClO. In addition to the FRS and the two
5 Ring spectra, we included SO_2, O_3, O_4, NO_2 and CH_2O into the fit.

Figure 3 shows an exemplary fit result of BrO ($S_{BrO} = 6.34 \times 10^{14}$ molecules cm^{-2}) and OClO ($S_{OClO} = 1.35 \times 10^{14}$ molecules cm^{-2}) and the corresponding fit residual (peak-to-peak value: $\overline{\Delta}_{res} = 1.18 \times 10^{-3}$).

In order to verify the retrieved OClO-SCDs and to assess possible influences of radi-
10 ation transport or cross correlations between different absorbers we defined a second evaluation range for OClO.

2.4.3 Alternative OClO evaluation routine (OClO^{uwr})

OClO was additionally evaluated in a second range between 363.6 and 391.3 nm covering three OClO absorption bands. Besides the two Ring spectra and the FRS, we
15 additionally included reference spectra of SO_2, O_3, O_4, NO_2. In principle, an advantage of this "upper" wavelength range should be, that it is less influenced by potential cross absorptions with BrO, O_3 or H_2CO. However, it was found that in most cases it showed distinct residual structures resulting in relatively large fit uncertainties compared to the previously described OClO range (see also Sect. 2.4.1, Stutz and Platt,
20 1996). These structures are most likely caused by distinctive solar Fraunhofer lines present in this wavelength range. These can cause a strong Ring effect which most likely cannot be fully described by the two included Ring spectra. A correlation plot of the retrieved OClO-SCDs for both evaluation ranges can be found in Fig. A1. We found a good correlation between both evaluation ranges for our dataset with slightly higher
25 values ($\approx 8\%$) for the SCDs from the upper range. For the discussion of our results, we

used the OClO data retrieved in the previously discussed wavelength range between 330.6 and 356.3 nm.

2.4.4 SO$_2$ evaluation routine

Cross section scans of volcanic plumes usually cover a large variety of SO$_2$-SCDs. While the SO$_2$-SCDs can reach values of several 10^{18} molecules cm^{-2} for light, which has traversed the centre of the plume, they decrease towards the edges of the plume until they reach values below the respective detection limit. The SO$_2$-detection limit of the instrument used in this study is of the order of 5×10^{16} molecules cm^{-2}. SO$_2$ shows distinctive broad- and narrowband absorption features in the wavelength range below 325 nm and is therefore usually evaluated between 300 and 325 nm (passive DOAS measurements). Tropospheric measurements below 300 nm are difficult using the passive DOAS method since almost no scattered sunlight is available due to the strong stratospheric O$_3$-absorption.

In case of strong SO$_2$ absorption (SO$_2$-SCDs of the order of several 10^{18} molecules cm^{-2}), the DOAS evaluation becomes problematic in the wavelength range between 300–325 nm due to radiation transport effects. These are discussed in detail by Kern et al. (2010) and Bobrowski et al. (2010), a brief description will be given in the following: high SO$_2$ column densities cause a strong variation in the accumulated photon light paths between local maxima and minima of the SO$_2$ cross section (σ_{SO_2}). This means, that the average effective absorption light path in the plume is likely to be shorter in wavelength regions located around local maxima of the SO$_2$ absorption cross section (σ_{SO_2}) compared to local minima. Therefore, we evaluated SO$_2$ in a second wavelength range between $\Delta\lambda_{SO_2}^{uwr} = 349.8$–372.8 nm in analogy to Hörmann et al. (2013). This range was used for SO$_2$-SCDs exceeding 3×10^{18} molecules cm^{-2}. For SO$_2$-SCDs below 3×10^{18} cm^{-2} we used the "standard" wavelength-range between $\Delta\lambda_{SO_2}^{lwr} = 314.8$–326.8 nm (e.g. Vogel, 2011) which is suited for small SO$_2$-SCDs for example from the edges of the plume or in aged plumes. Details

on the two SO_2 fitting-routines can be found in Table 1. A correlation plot of the retrieved SO_2-SCDs for the two fit-ranges is shown in Fig. A2. The plot shows clearly, that the retrieved SCDs are underestimated in the lwr-range in case of large SO_2-SCDs (i.e. $S_{SO_2} > 3 \times 10^{18}$ molecules cm^{-2}). For smaller SCDs we found a good correlation with an increased scattering in the uwr-range in case of low SCDs (due to the small SO_2-absorption cross section in this range).

2.4.5 Evaluation ranges for IO, OIO and OBrO

In addition to the evaluation of BrO, OClO and SO_2, we also evaluated the spectra for IO, OBrO, and OIO. Shift and squeeze settings for the corresponding evaluation-routines follow the previously described general settings as does the included Ring spectra ($R, R4$). The other parameters for the evaluation routines of IO, OIO and OBrO (i.e. wavelength range, additionally fitted species σ_i) are given in Table 1. The table summarises all DOAS fitting-routines used in this study. All literature cross sections (σ_i) used in this study are summarised in Table 2.

2.5 Estimation of OClO and BrO concentrations from plume cross section scans

In order to derive mean concentrations ($\bar{c}_i$) from the retrieved SCDs (S_i), we estimated the length of the effective absorption light paths in the plume ($l_{eff,i}$).

By assuming a circular plume shape, the effective plume diameter ($\varnothing_{pl}$) can be estimated from the angular extend of the SO_2-SCD profile (derived from plume cross section scans), provided that the distance to the plume is known (see also e.g. Bobrowski et al., 2003; Lee et al., 2005). The plume distance was estimated using the meteorological data and the geo-coordinates of the instrument and the active crater region.

Assuming that $\varnothing_{pl}$ corresponds to the effective absorption length of the spectrum with the largest SO_2-SCD (i.e.: $l_{eff,0}(S_{SO_2,max}) = \varnothing_{pl}$), we determined the absorption lengths

$l_{\text{eff},i}$ of all scan-spectra i in the following way:

$$l_{\text{eff},i} = \frac{S_{\text{SO}_2,i}}{S_{\text{SO}_2,\text{max}}} \cdot l_{\text{eff},0}. \tag{2}$$

Using this, mean concentrations ($\bar{c}_{j,i}$) of the measured species j (e.g. OClO, BrO) can be estimated as follows:

$$\bar{c}_{ji} = S_{j,i}/l_{\text{eff},i}. \tag{3}$$

We want to emphasize, that the determined values are rather an estimate of the order of magnitude of the concentrations since we assumed a circular plume shape ($l_{\text{eff},0} = \varnothing_{\text{pl}}$) and did not consider any radiation transport effects (e.g. multiple scattering in the plume, see e.g. Kern et al., 2010).

2.6 Determination of ClO concentrations

Following Kern et al. (2009), we estimated ClO concentrations from the retrieved BrO and OClO-SCDs assuming steady state between the formation of OClO (R6) and its photolytic destruction (R7):

$$\text{ClO} = \frac{J_{\text{OClO}}}{k_1} \cdot \frac{[\text{OClO}]}{[\text{BrO}]} \approx \frac{J_{\text{OClO}}}{k_1} \cdot \frac{S_{\text{OClO}}}{S_{\text{BrO}}} \tag{4}$$

Since BrO and OClO were evaluated in the same wavelength range, differences in the retrieved SCDs (S_i) due to radiation transport effects can be neglected. We therefore assume, that the ratio of the OClO and BrO concentrations is approximately the same as the ratio of the respective SCDs (Eq. 4). The OClO photolysis frequencies J_{OClO} used for the calculation of the ClO concentrations were simulated for our dataset by E. Jäkel (Leipzig Institute for Meteorology). For the simulation, the 1-D radiative transfer model libRadtran (Mayer and Kylling, 2005) was used. The photolysis frequencies were

determined for a set of chosen spectra from the field campaign and lie between $5.1 \times 10^{-2}\,\mathrm{s}^{-1}$ (SZA $\approx 62°$) and $7.1 \times 10^{-2}\,\mathrm{s}^{-1}$ (SZA $\approx 34°$), slightly slower compared to the stratospheric OClO-photolysis of $J_{\mathrm{str,OClO}} \approx 7.6 \times 10^{-2}\,\mathrm{s}^{-1}$, published by Birks et al. (1977).

2.7 Determination of the plume age (τ) and meteorological data

2.7.1 Algorithm and error representation

The plume age (τ) was estimated for each spectrum using meteorological information (i.e. wind speed and direction) and the measurement geometry (i.e. geo-locations of instrument and craters, telescopes viewing direction). Figure 4 shows a sketch of a typical measurement geometry at Mt. Etna. The plume age τ was estimated using the following equation:

$$\tau = \frac{l}{v_{\mathrm{wind}}} \tag{5}$$

whereas l accounts for the horizontal distance of a given point P to the emission source P_0[2]. A good knowledge of the meteorological data (i.e. wind velocity and direction and the corresponding uncertainties) is therefore indispensable to retrieve a good estimation of τ. The distance l can be determined from both the geo-locations of the instrument (Fig. 4, P_D) and the emission source (Fig. 4, P_0) and from the respective orientations of plume (δ) and telescope (α). We used a simple geometrical approach to determine the intersection point of the plume with the telescopes viewing direction (P) from these parameters.

A good estimate of τ is of particular importance for the interpretation of the data gathered in the plume evolution scans (for details see Sect. 2.3). For these scans, τ

---

[2]This assumption is only valid when horizontal transport (i.e. wind driven) dominates such that vertical plume propagation (e.g. convective rise) can be neglected. This was the case for all data collected during this campaign due to high wind velocities.

increases between the individual scan-spectra since the scan is performed along the plume propagation axis.

2.7.2 Uncertainties and simplifications

The main uncertainties of the plume age determination using Eq. (5) are due to uncertainties in the wind velocity and the determination of l (i.e. mainly reducible to uncertainties in δ and α, see Fig. 4). We thus subdivided our error-representation of τ into two contributions:

1. The first (in the following denoted as $\Delta\tau_l(\alpha, \delta)$) is determined from the uncertainties in α and δ (mainly geometrical uncertainties). $\Delta\tau_l(\alpha, \delta)$ can vary strongly between different spectra from plume evolution scans due to the nature of the trigonometric functions involved in the calculation of l. $\Delta\tau_l(\alpha, \delta)$ is therefore plotted for each spectrum separately in form of x axis error bars (see e.g. Fig. 8).

2. The second contribution (in the following denoted as $\Delta\tau_{v_{wind}}$) to the plume age error is caused by uncertainties in the wind velocity Δv_{wind} and has a rather linear dependency with respect to $\Delta\tau$ ($\partial\tau/\partial v_{wind} \propto \Delta v_{wind}$). Since $\Delta\tau_{v_{wind}}$ is independent of the measurement and plume angles, its relative impact on each spectrum ($\Delta\tau_{v_{wind}}/\tau$) is constant. The corresponding contribution is therefore given as a percentage value in the plot header (denoted as $\Delta\tau$, e.g. see Fig. 8).

For simplicity, we reduced the determination of τ to a 2-D problem in the horizontal plane, because for typical scanning geometries (and a wind driven, horizontal plume propagation), differences in the altitude between plume and DOAS instrument have only a small influence on the determination of τ.

Furthermore, by reducing the volcanic plume and the telescopes viewing direction to a line (dotted lines in Fig. 4) we did not consider any effects caused by plume dispersion or the telescopes field of view for our estimation of τ. These effects are usually negligible for typical scan geometries ($\varphi \approx 90°$, see Fig. 4) and may be considered when

the measurements are performed at small angles φ. In this case the analysed light has penetrated a multiple of different plume ages which essentially causes a smoothing of the signal with respect to τ. The corresponding impact with regard to the data interpretation depends on the desired temporal resolution of the respective scan (i.e.
$\Delta\tau$ between individual scan spectra) and on the chemical variability of the analysed species in the analysed plume age range.

A further simplification in our algorithm is the reduction of the four main craters (BN, VOR, NE and SE) to a single emission source point P_0 (i.e. $\tau = 0$ point) located at 37°45′6.7″ N, 14°59′49.6″ E between the central craters (BN, VOR) and NE.

Furthermore, chemical processes which may have taken place already within the craters are also not considered in our routine. The latter effect can cause a plume age offset with respect to P_0. Both effects are strongest for viewing directions close to the vent were the plumes are still separated. However, in most cases the corresponding error was assessed to be relatively small considering the uncertainties in the meteorological data.

2.7.3 Geometrical and meteorological data

The azimuthal alignment of the instrument was performed using a compass. Due to possible disturbances of the planetary magnetic field by the volcano, we estimated the instruments azimuth-uncertainty to ±3° (gray shaded area in Fig. 4). During the first three days, the wind directions and velocities were determined partly from simultaneously performed SO_2-camera measurements and from own observations/notes. In addition, images from the MODIS satellites Aqua and Terra were used to specify wind directions. This was possible during cloud free conditions, when the condensed volcanic plume could be detected in the satellite images. From the 16 September we additionally monitored meteorological data using a meteorological station, which was installed on the southern side of the craters. These data was used to improve our estimate of wind direction and velocity by inter-comparison with the satellite data, own observations and the SO_2-camera data. Due to geometrical and meteorological uncertainties,

OCIO and BrO observations in the volcanic plume of Mt. Etna

Gliß et al.

Full Screen / Esc

Printer-friendly Version

Interactive Discussion

the respective τ-errors became considerably large in some cases. This was especially the case when the meteorological data was not well known and/or the angle between the telescopes viewing direction and the plume propagation direction was small. However, we want to point out that these uncertainties in the absolute value of τ are not to be treated as random errors between individual scan-spectra but rather act as a τ-shift towards smaller or larger plume ages (i.e. "stretching" or "squeezing" of the plume).

2.8 Correction for stratospheric BrO

Typical vertical column densities (VCDs) of stratospheric BrO are of the order of several 10^{13} molecules cm^{-2} (e.g. Schofield et al., 2004; Sinnhuber et al., 2005). MAX-DOAS measurements of volcanic BrO (using scattered sunlight) can be significantly disturbed by stratospheric BrO signals under certain conditions. The impact is largest at large zenith angles (i.e. in the morning and afternoon hours).

The BrO-SCDs (S_{meas}) derived from the DOAS evaluation (see Sect. 2.4) are composed of a volcanic (S_{plume}) and a stratospheric contribution (dS_{str}). The latter is due to changes in the zenith angle (Θ) between plume spectrum and FRS.

$$S_{plume} = S_{meas} - dS_{str} \qquad (6)$$

In order to examine dS_{str}, we used a simple geometrical approach assuming, that the air-mass-factor (AMF) is given by the inverse cosine of Θ: AMF $= 1/\cos(\Theta)$ (see also Hönninger et al., 2004). For our purposes, this assumption was assessed to be sufficient, since plume spectra and FRS were recorded close in time and the SZAs were in most cases (99.1 %) smaller than 80°. For a more accurate estimation of the AMF, radiative transfer calculations are necessary.

The total stratospheric column $S_{str,i}$ for a given spectrum i can then be calculated from its stratospheric vertical column V_{str} using the following relation: $S_{str,i} = V_{str}/\cos(\Theta_i)$. Based on this, the corresponding stratospheric contribution d$S_{str,ij}$

OCIO and BrO observations in the volcanic plume of Mt. Etna

Gliß et al.

between two spectra i, j can be determined in the following way:

$$dS_{str,ij} = V_{str} \cdot \left(\frac{1}{\cos(\Theta_i)} - \frac{1}{\cos(\Theta_j)} \right) \overset{\text{def}}{=} V_{str} \cdot \gamma_{ij}. \tag{7}$$

Inserting Eq. (7) into Eq. (6) yields the following relation for the corresponding volcanic BrO column:

$$S_{plume} = S_{meas} - V_{str,BrO} \cdot \gamma_{ij}. \tag{8}$$

We estimated $V_{str,BrO}$ by applying the DOAS evaluation of BrO (see Sect. 2.4.2) to a set of spectra recorded out of the plume and at large SZAs (i.e. from morning and afternoon hours). These were evaluated against plume free spectra (i.e. FRS) performed at small SZAs around noon to retrieve $dS_{str,ij}$ and from that, $V_{str,BrO}$ was derived using Eq. (7). The VCDs were between $V_{str,BrO} = 2.9 \times 10^{13}$–$7.2 \times 10^{13}$ molecules cm^{-2}, the corresponding SZAs between 33.7–70.1° respectively. These values are in good agreement with the findings of Sinnhuber et al. (2005). According to Schofield et al. (2004) large diurnal variations in the stratospheric BrO-column are unlikely for the SZA range covered by our dataset ($\Theta < 83°$). We therefore assumed a constant stratospheric BrO amount of $V_{str,BrO} = 4.0 \times 10^{13}$ molecules cm^{-2} and applied a correction to our retrieved BrO-SCDs using Eq. (8). Sinnhuber et al. (2005) and Schofield et al. (2004) measured stratospheric vertical columns in the range of 2–4 $\times 10^{13}$ molecules cm^{-2}. Our correction factor ($V_{str,BrO}$) was chosen at the upper end of this scale in best agreement with our results (2.9–7.2 $\times 10^{13}$ molecules cm^{-2}). The impact of the stratospheric signals on our BrO retrieval is visualised in Fig. 5. We plotted the relative amount of stratospheric BrO with respect to the measured SCDs (i.e. dS_{str}/S_{meas}) as a function of the parametrisation factor γ_{ij} (see Eq. 7). We included all spectra of our dataset showing a significant BrO-SCD and found that the deviations due to the superimposed stratospheric BrO signal are smaller than 5% for 85% of the analysed spectra. Only 8% of the retrieved BrO-SCDs showed significant deviations according to the respective

measurement uncertainty (see Sect. 2.4.1). All of these spectra were either recorded before 08:15 LT or after 16:45 LT ($64.6° <$ SZA $< 83.2°$).

Of course, the relative impact of the stratospheric contribution increases for smaller measured BrO-SCDs (compare e.g. dark blue with green colours in Fig. 5). For BrO-SCDs of the order of 6×10^{14} molecules cm^{-2} (green colours) we found that the impact of dS_{str} on the measured signal amounts to $a = 6.6\,\%/\gamma_{ij}$ (linear regression in Fig. 5). To estimate the influence of variations in the total stratospheric BrO load ($V_{str,BrO}$), we additionally determined this slope for two different stratospheric BrO-VCDs of $V_{str,BrO} = 2 \times 10^{13}$ and $V_{str,BrO} = 7 \times 10^{13}$ molecules cm^{-2}.

The corresponding slopes were found to be $a = 3.4\,\%/\gamma_{ij}$ and $a = 11.8\,\%/\gamma_{ij}$ respectively. This shows, that the impact of stratospheric BrO is in most cases small (i.e. for small γ_{ij}-values), even for considerably high stratospheric VCDs. Nonetheless, one has to keep in mind, that these slopes were determined for relatively high BrO-SCDs of the order of $S_{meas} = 6 \times 10^{14}$ molecules cm^{-2}. For lower measured BrO-SCDs (S_{meas}, blue colours in Fig. 5), the impact of stratospheric BrO increases and can significantly influence the volcanic signal, especially at large differences in the SZA (i.e. large γ_{ij}-values).

2.9 SO$_2$ as volcanic plume proxy

Tropospheric SO$_2$ has a comparatively long lifetime of several hours up to days (e.g. McGonigle et al., 2004; Lee et al., 2011; Beirle et al., 2014) and can therefore be treated as a passive tracer. In order to analyse the spatial distribution and temporal evolution of the measured halogen species (X_mO_n), we studied the ratio of these species with the retrieved SO$_2$-SCDs: X_mO_n/SO$_2$-ratio (e.g. Bobrowski et al., 2003; Bobrowski and Platt, 2007; Bobrowski et al., 2007; Kern et al., 2009). This representation has the great advantage, that atmospheric dilution effects on the retrieved SCDs cancel out.

3 Results and discussion

Due to the improved sensitivity of the instrument it was possible to detect OClO in 119 individual spectra during the field campaign in September 2012. Most of these spectra were recorded during the first three days of the campaign at the Etna ob-
servatory which is located close to the volcanic craters (ca. 2.5 km distance). At the observatory the measurements are mostly performed in the young plume (i.e. $\tau < 5$ min) were plume dispersion is in an early stage and the retrieved SCDs are therefore comparatively large. OClO could be detected up to plume ages of six minutes after release. BrO was detected in 452 spectra at plume ages up to 23 min,
the mean OClO/BrO-ratio was 0.16. The retrieved SCDs of OClO, BrO and SO_2 ranged between 0.4–2.0 × 10^{14} molecules cm^{-2}, 0.3–11.4 × 10^{14} molecules cm^{-2} and 0.03–8.77 × 10^{18} molecules cm^{-2} respectively (i.e. for measurements above the detection limit, see Sect. 2.4.1). Furthermore, the evaluation of IO and – making use of the extended wavelength range of the instrument – OIO and OBrO was investigated but
none of these species could be detected in the retrieval. However, upper limits of IO, OIO and OBrO were determined for two different plume age ranges (for details see Sect. 3.2).

In the following section the results of the OClO and BrO retrieval are presented.

3.1 OClO and BrO results

Figure 6 shows all retrieved OClO and BrO-SCDs as a function of the corresponding SO_2-SCDs (A, B) and the retrieved OClO-SCDs as a function of the BrO-SCDs (C). In this representation we only included measurements showing significant SO_2 detections (see also Sect. 2.4.1).

The plots (Fig. 6) show that for all plume ages both BrO and OClO could only be detected within the plume (i.e. linear correlation with SO_2). For plume ages larger than three minutes (blue dots) we found average ratios of 1.55 × 10^{-4} (BrO/SO_2) and 3.17 × 10^{-5} (OClO/SO_2). For the linear regression of BrO (A) and OClO (B, C),

measurements below the respective detection limit (red dots in Fig. 6) as well as measurements performed at plume ages smaller than three minutes (green stars) were excluded. The latter was done because the formation of BrO and OClO is yet not fully developed in this plume age range (for details see Sect. 3.1.3) and therefore the X_mO_n/SO_2-ratios are smaller (see e.g. Fig. 7). The average BrO/SO_2 and OClO/SO_2-ratios are in good agreement with previous studies at Mt. Etna (e.g. Bobrowski et al., 2007; Bobrowski and Giuffrida, 2012; General et al., 2014). Figure 6c shows a good correlation (R^2 = 0.9447) between BrO and OClO for plume ages larger than three minutes with a mean OClO/BrO-ratio of 0.16 ± 0.08. The measurements performed in the young plume (green dots, $\tau < 3$ min) rather indicate a stronger fluctuation (R^2 = 0.4717) of the OClO/BrO-ratio.

3.1.1 Scan example and discussion of the retrieved uncertainties

In Fig. 7 an exemplary plot of a plume evolution scan of the OClO/SO_2-ratio is shown. As discussed in Sect. 2.7 the errors in the plume age are separated into a geometrical contribution (x-error bars) and a percentage contribution due to uncertainties in the wind velocity ($\Delta\tau$, see plot header). We point out again, that these errors are not to be treated as independent random uncertainties between each of the scan spectra. They rather indicate a shift of the whole dataset towards smaller or larger plume ages.

Figure 7 shows an increase of the OClO/SO_2-ratio up to a plume age τ of approximately 120 s and a slight decreasing trend afterwards. This decrease can not be explained at this point but it is still in the range of the natural fluctuations we observed for this plume age range ($\tau < 2$ min, see Fig. 6). The uncertainties in the ratios are comparatively large, but – similar to the plume age determination – are also not to be treated as random errors since they also include systematic errors. This means basically, that the uncertainty of any X_mO_n/SO_2-ratio represented in the error bars is rather an absolute uncertainty for all spectra, hence, that the whole dataset might be shifted towards higher or lower ratios. However, relative values and especially trends between individual scan spectra are still relevant even if they are partly below the detection limit

of an individual measurement as is the case here. We would also like to remark that there are a total of 10 data points showing a consistent behaviour.

3.1.2 Cross sectional distribution of BrO and OClO

In order to study variations of BrO/SO_2 and $OClO/SO_2$ between the centre of the plume and its edges we performed plume cross section scans perpendicular to the plume propagation axis (see Fig. 2b). Previous studies indicated an increase of the BrO/SO_2 ratio towards the edges of the plume (e.g. Bobrowski et al., 2007; Louban et al., 2009; General et al., 2014).

The higher BrO/SO_2-ratio near the plume edge is likely due to the limited transport of tropospheric ozone O_3 and HO_2 radicals towards the plume centre (see also Sect. 1.1). A typical cross-section scan of the BrO/SO_2-ratio is shown in Fig. 8f with a scan time of approximately 36 min. In this example, 1000 spectra were co-added at each measurement position and the spatial angular resolution (x axis) was 4°. The average integration time was $\Delta t_{meas} = 2.5$ min per spectrum. The plume profile is defined by the SO_2 profile of the scan. The low temporal resolution caused by adding a large number of spectra sequentially recorded over the spatial plume extension has some disadvantages, for example: variations in the wind direction, the emission strength or the plume rise during a scan could cause a blurring of the plume profile. Nonetheless, it was still possible to examine changes of the X_mO_n/SO_2-ratio from MAX-DOAS scans by analysing the retrieved ratio as a function of the corresponding SO_2-SCD. Figure 8f shows a typical SO_2 plume profile with a maximum around 30°-elevation ($S_{SO_2,max} = 1.9 \times 10^{18}$ molecules cm^{-2}). The corresponding BrO/SO_2-ratio is almost constant ($\sim 2.0 \times 10^{-4}$) for SO_2-SCDs of the order of 10^{18} molecules cm^{-2}. For smaller SO_2-SCDs (i.e. at the plume edge) we observed slightly elevated values, in fact the largest BrO/SO_2-ratios were found at lowest SO_2-SCDs (i.e. 59° and 70° telescope elevation).

OClO and BrO observations in the volcanic plume of Mt. Etna

Gliß et al.

In order to further analyse the cross-sectional profile of BrO/SO_2 (and $OClO/SO_2$) we performed a statistical analysis of all cross section scans which are suited in terms of their SO_2-plume coverage. With respect to a certain SO_2-SCD threshold (in the following denoted as SO_2-Lim) we subdivided the plume into a "plume-centre" and a "plume-edge"-range for each scan. All scan spectra with $SO_2 > SO_2$-Lim were assigned to the "plume-centre", all others to the "plume-edge". For this study, SO_2-Lim was defined to be 50 % of the maximum SO_2-SCD detected in the respective scan. We only considered scan spectra showing a significant SO_2-SCD for this analysis.

Using these parameters, we then studied mean percentage changes in the X_mO_n/SO_2-ratio between plume-centre and plume-edge by analysing the ratio R which is defined as follows:

$$R = \frac{\overline{(X_mO_n/SO_2)_{edge}}}{\overline{(X_mO_n/SO_2)_{centre}}} \tag{9}$$

We examined R in two different ways: the corresponding values are denoted as R_{ALL} (all spectra) and R_{AD} (X_mO_n-SCDs above the detection limit). The results of this study can be found in Table A1 with the retrieved R_{AD} and R_{ALL} values which were converted to percentage representation (AD, ALL). Additional information and further details on the evaluation algorithm are also provided in Table A1.

Results for BrO

The BrO/SO_2 ratio showed an increase towards the edges in 76 % of all analysed scans. On average, the ratios were enhanced by $\overline{AD} = 30 \pm 18$ % and $\overline{ALL} = 37 \pm 33$ % respectively in the "edge"-range. 16 % of the analysed scans indicated a decreasing trend towards the edges. For 8 % of the scans no clear trend was observable due to discrepancies between the retrieved AD and ALL values.

Results for OClO

The corresponding results for $OClO/SO_2$ are unfortunately not as clear as in case of BrO since the $OClO/SO_2$-ratio was always below the detection limit in the "edge"-range. We were therefore not able to determine R_{AD} values for any of the nine suited scans (see A1, subtable 2). However, five of these scans indicate elevated $OClO/SO_2$-ratios at the edges of the plume, showing R_{ALL}-values between 10 and 250 %. The large variability in the R_{ALL}-values is probably due to the weak OClO signal in the edge range, the limited amount of measurements does not provide enough data for a statistical approach. Two of the nine analysed scans indicated a decrease of the $OClO/SO_2$-ratio at the edges.

However, it is plausible that – besides BrO/SO_2 – also the $OClO/SO_2$-ratio is elevated at the edges when assuming that OClO is formed via the "BrO + ClO"-reaction (provided that enough ClO is available at the edges).

3.1.3 The BrO and OClO evolution in the plume

We observed an increase of BrO/SO_2 and $OClO/SO_2$ in the young plume ($\tau \lesssim 3\,\mathrm{min}$) and a levelling off at larger plume ages. This increase was observed in six individual measurements (i.e. plume evolution scans, see Sect. 2.3) performed in the young plume (i.e. $\tau < 5\,\mathrm{min}$) and could be confirmed in an additional statistical analysis of our retrieved results in this plume age range (see also Table 3). Some exemplary plume evolution scans are presented in Fig. 8 showing the increase in the young plume (Fig. 8a, d) for BrO/SO_2 and $OClO/SO_2$ respectively.

In case of $OClO/SO_2$ (Fig. 8d) all retrieved values are below the detection limit. However, as already discussed in Sect. 3.1.1, the increasing trend is still reasonable since relative errors between individual scan spectra are smaller. Furthermore, this trend was also observed during other measurements performed in this plume age range (e.g. Fig. 7, for details see Table 3).

Figure 8b shows an intermediate plume age range (2.1–3.4 min) with a rather constant BrO/SO_2-ratio of 1.4×10^{-4}. The corresponding values for the $OClO/SO_2$-ratio (Fig. 8e) indicate an steady state after $\tau_{0,OClO} = 2.25$ min. In addition, BrO could also be analysed for larger plume ages (i.e. $\tau > 5$ min) due to its higher S/N-ratio. An exemplary BrO scan in the aged plume is shown in Fig. 8c. It covers a range between 8 and 22 min downwind and shows rather stable BrO/SO_2-ratios around 1.7×10^{-4}. Between eight and ten minutes downwind, a slight decrease of approximately 17 % is observable. This could be a result of a superimposed vertical profile of BrO. Due to plume dispersion, the SO_2-SCDs should decrease with increasing plume-age. This is not observable in this example (i.e. Fig. 8c), the corresponding SO_2-SCDs show rather constant values around 5×10^{17} molecules cm^{-2}. It is thus possible that the scan axis was slightly misaligned with respect to the plume propagation axis. This would mean that the first spectra of the scan shown in Fig. 8c (large BrO/SO_2-ratios) may have been recorded off the plume centre. This is further supported by the plume-cross-section scan shown in Fig. 8f which was performed directly before Fig. 8c at $\tau = 6$ min. The corresponding SO_2-profile indicates plume-centre-SCDs of the order of several 10^{18} molecules cm^{-2} for this plume age regime (6–8 min).

The retrieved BrO/SO_2-ratios in the $\tau > 3$ min-regime (i.e. after reaching steady state, see Fig. 8a–c) vary between 8×10^{-5} to 1.8×10^{-4}. Reasons for that could be variations in the volcanic activity or superimposed diurnal profiles (note: the scans were performed at different days and times).

Increasing BrO/SO_2-ratios in the young plume were already observed in other studies (e.g. Bobrowski et al., 2007). In case of OClO it is the first observation of its formation. The similarities to our BrO observations (i.e. increase in the young plume and steady state after about 2–3 min) support the assumption that most of the OClO is formed via the "BrO+ClO"-reaction (R6).

Statistical analysis of the young plume evolution

In order to further elaborate the observed increase of BrO and OClO in the young plume we made a statistical analysis of the retrieved X_mO_n/SO_2-ratios as a function of the plume age. For this study, we subdivided the young plume into six intervals considering only plume ages between zero and 250 s (i.e. ~ 42 s interval^{-1}). Based on this, our retrieved X_mO_n/SO_2-ratios were assigned to the respective plume age interval. We only considered spectra related to the plume-centre by including only measurements showing SO_2-SCDs larger than 1.5×10^{18} molecules cm^{-2} (see also Sect. 3.1.2). We did not distinguish between measurements above or below the respective detection limits of BrO and OClO. Based on this selection, we determined the mean-value of the retrieved X_mO_n/SO_2-ratios for each τ-interval. The results are shown in Fig. 9. The corresponding uncertainties (Δ, i.e. y axis errors) for the averaged ratios were determined from the mean of the individual errors ($\overline{\sigma_i}$) divided by the inverse square-root of the number N of averaged spectra in each interval: $\Delta = \overline{\sigma_i}/\sqrt{N}$.

The results of this statistical approach clearly show the increase of BrO/SO_2 and $OClO/SO_2$ in the young plume, confirming our observations from the individual plume-evolution scans (see previous section). Both BrO/SO_2 and $OClO/SO_2$ level off after approximately 142 s. However, while BrO/SO_2 reaches a constant plateau of $\sim 1.3 \times 10^{-4}$ at larger plume ages, the $OClO/SO_2$-ratio rather seems to follow a slight decreasing trend. Indications of such a decrease could also be observed in some of the individual scans (compare e.g. Fig. 7).

The retrieved BrO/SO_2 and $OClO/SO_2$-ratios for the plume age range after levelling off (i.e. $\tau > 142$ s) are slightly lower compared to the values retrieved in the corresponding scatter plots of the whole dataset (i.e. $\overline{BrO/SO_2} = 1.55 \times 10^{-4}$, $\overline{OClO/SO_2} = 3.17 \times 10^{-5}$, see Fig. 6). One explanation for this deviation could be, that spectra related to the plume-edges (which showed elevated BrO/SO_2 and $OClO/SO_2$-ratios, see Sect. 3.1.2) were excluded in the statistical approach. Further possible reasons could be that the long term trend of both species (i.e. $\tau > 250$ s) is still increasing or

OClO and BrO observations in the volcanic plume of Mt. Etna

Gliß et al.

Title Page

Abstract	Introduction
Conclusions	References
Tables	Figures

|◄ | ►|

◄ | ►

Back | Close

Full Screen / Esc

Printer-friendly Version

Interactive Discussion

that a superimposed diurnal signal might have influenced the statistics. Moreover, both long and short-term variations of the volcanic activity might have affected the retrieved ratios. Nonetheless, the main objective of this study, namely the young plume increase of both species could be validated. In order to further elaborate the long term trend of BrO and OClO (and/or diurnal profiles, variations due to volcanic activity) more measurements are necessary, especially for plume ages larger than $\tau < 250\,s$.

Table 3 gives an overview of the retrieved formation times (τ_0) of BrO and OClO, meaning the plume ages, where BrO/SO_2 and $OClO/SO_2$ start levelling off. The last column (Δ) indicates the difference in the formation duration of OClO and BrO (i.e. $\Delta = \tau_{0,OClO} - \tau_{0,BrO}$). From the individual scans (i.e. rows 1–6) it appears that the BrO formation reaches its steady state slightly faster compared to OClO. While $\tau_{0,BrO}$ ranged from 24–154 s, the OClO formation lasted about 70 % longer with values of $\tau_{0,OClO}$: 85–226 s (rows 2–6). Only a single plume scan showed similar formation times for both species (row 1, $\tau_0 \approx 123\,s$) as did our statistical analysis (row 7, $\tau_0 \approx 142\,s$, see also Fig. 9). Since BrO and ClO are most likely the chemical precursors of OClO, it is in principle possible that the formation duration of OClO is longer compared to BrO. The variations in the formation times itself could be caused by uncertainties in the plume age determination (for details see Sect. 2.7) but could also indicate a variability in the effectiveness of the reaction mechanisms involved.

3.1.4 Photochemical formation of BrO and OClO

As explained in Sect. 1, the BrO formation is probably driven by the "bromine explosion" a reaction mechanism which includes the photolysis of the Br_2-molecule (for details see Sect. 1). Kern et al. (2009) investigated night time abundances of BrO at Masaya volcano Nicaragua and were not able to detect significant BrO levels during night-time. Although MAX-DOAS measurements can only be made when sunlight is available, we were able to observe the onset of the BrO and OClO formation during a point measurement (for details see Sect. 2.3) in the early morning with little availability of scattered sunlight. The measurement was performed between 05:20 and 06:20 UTC on the

Title Page

Abstract | Introduction

Conclusions | References

Tables | Figures

|◄ | ►|

◄ | ►

Back | Close

Full Screen / Esc

Printer-friendly Version

Interactive Discussion

13 September (SZA-range: 83.2–70.1°, sunrise: 04:40 UTC) and showed an increase of the BrO/SO$_2$-ratio with time between 05:20 and 05:32 UTC (top) (see Fig. 10) and a levelling off afterwards. The corresponding SO$_2$-profile is fairly constant with typical plume centre values around 5×10^{18} molecules cm^{-2}. This shows that the measure-
5 ment conditions (e.g. wind direction and velocity) did not change significantly during the measurement. Making this trend (at large SZAs) visible was only possible due to our correction algorithm for stratospheric BrO signals (see Sect. 2.8). We therefore attribute the increase in S_{BrO} to be a result of the increasing solar irradiance after sunrise. This is further evidence that the availability of sunlight is an important parameter for the
10 formation of BrO in volcanic plumes, underpinning the theory of the bromine-explosion. For the corresponding OClO/SO$_2$-ratio no clear inferences can be drawn due to rather large uncertainties (only the last 5 points are above the DOAS detection limit). However, having in mind the extensive discussion about relative and random errors between individual DOAS-measurements (see Sects. 2.4.1 and 3.1.3), an increase of the
15 OClO/SO$_2$-ratio might also be observable here. Until 06:05 UTC, the values are below the detection limit varying slightly with a mean OClO/SO$_2$-ratio of 1.20 ± 0.25. They follow a short increasing trend afterwards and seem to reach a plateau around 06:14 UTC (last five datapoints) with a mean abundance of 1.79 ± 0.39. This observation indicates that the OClO formation in the early morning might be delayed with respect to BrO
20 (approximately 40 min). One possible explanation for such a delayed increase could be that the availability of Cl-atoms is delayed with respect to Br during this time of day (since OClO is likely formed via the "BrO + ClO"-reaction and BrO and ClO via reaction of Br and Cl with O$_3$). However, this hypothesis is rather speculative due to the large uncertainties in the OClO retrieval and further studies are necessary to prove or
25 refute this. Another point measurement performed on the 22 September 2012 later in the morning (06:33–06:48 UTC, $\tau = 7.6 \pm 1.6$ min) showed a stable BrO/SO$_2$-ratio of $(1.15 \pm 0.2) \times 10^{-4}$ (20 spectra). This is in good agreement with the values shown in Fig. 10 after reaching the steady state (past 05:30 UTC).

3.1.5 Retrieved BrO, OClO and ClO mixing ratios

As described in Sect. 2.5 we determined BrO and OClO concentrations from the retrieved SCDs by estimating the effective absorption length $l_{\text{eff},i}$ for all spectra with sufficiently high S/N-ratios. The corresponding results are plotted in Fig. 11 as a function of the plume age τ. We furthermore included the calculated ClO concentrations (see Sect. 2.6).

We retrieved BrO concentrations at plume ages between zero and 17 min with values between 36 ppt and 2.7 ppb whereas the highest values are found in the young plume. With increasing plume age the concentrations decrease due to plume dispersion. The derived OClO and ClO concentrations were between 37 and 597 ppt (OClO) and 70–235 ppt (ClO) covering plume ages up to six minutes downwind. Mean abundances in the young plume (i.e. $\tau < 4$ min) were $\overline{\text{ClO}} = 139 \pm 39$ ppt, $\overline{\text{BrO}} = 1.35 \pm 0.45$ ppb and $\overline{\text{OClO}} = 300 \pm 90$ ppt.

The measurements performed at the Etna observatory (i.e. $\tau < 4$ min) revealed a mean OClO/ClO-ratio of 2.16 ± 0.89. The only available data point for OClO and ClO at larger plume ages (i.e. $\tau = 6$ min, see Fig. 11) rather indicates an OClO/ClO-ratio of only 0.25. This deviation might merely be due to the relatively high uncertainty of this data point (i.e. OClO = 37 ± 24 ppt, ClO = 136 ± 99 ppt). Moreover, uncertainties in the plume-shape estimation could have affected the different results between the two measurement locations (i.e. due to deviations from the assumed circular shape, see Sect. 2.5). Nonetheless, these differences could still be indicating a "true" decrease of the OClO/ClO-ratio with increasing plume age (e.g. due to plume dispersion). However, not too much attention should be paid to this since it is only a single measurement showing such a comparatively low OClO/ClO-ratio and more measurements are necessary to investigate this issue further.

3.1.6 Estimation of Cl atom concentrations and a potential depletion of CH_4 in the plume

High abundances of chlorine atoms could cause a significant depletion of atmospheric methane (CH_4) in the plume environment. Once Cl atoms are produced (from oxidation of chloride) they can react with CH_4 forming HCl:

$$Cl + CH_4 \rightarrow HCl + CH_3. \tag{R8}$$
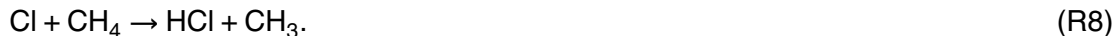
The reaction rate coefficient of R8 is $k_8 = 1.0 \times 10^{-13}\,cm^3\,s^{-1}$ at 298 K (16 times faster than the $OH + CH_4$ reaction at 298 K) and has a strong temperature dependence (Sander et al., 2006). Alternatively the Cl atoms can react with ozone:

$$Cl + O_3 \rightarrow ClO + O_2. \tag{R9}$$

The corresponding reaction rate coefficient is $k_9 = 1.2 \times 10^{-11}\,cm^3\,s^{-1}$ (298 K, Sander et al., 2006). All other reactions are much slower and are therefore neglected here.

Cl atom concentrations in the plume were estimated using the ClO and OClO concentrations inferred from our measurements (see Sect. 3.1.5) and the corresponding young plume formation times τ_0 (see Sect. 3.1.3). For the estimation we assumed that the total amount of ClO_y (i.e. $[ClO_y] = [ClO] + [OClO]$), observed after the levelling of OClO (i.e. at plume age τ_0, see also Sect. 3.1.3) was produced from Cl atoms via R9 (ClO) and further R6 (OClO). Assuming a linear increase of $[ClO_y]$ the corresponding rate of formation of Cl atoms was estimated as follows:

$$\left(\frac{d}{dt}[Cl]\right)_{obs} \approx \frac{d}{dt}[ClO_y] \approx \frac{[ClO_y]}{\tau_0}. \tag{10}$$

Actually the true rate of Cl atom production d/dt[Cl] is larger since a fraction of the Cl atoms reacts with CH_4 (R8) and never shows up as ClO_y (possible reaction of Cl with other hydrocarbons is likely to be unimportant and therefore neglected here):

$$\frac{d}{dt}[Cl] \approx \left(\frac{d}{dt}[Cl]\right)_{obs} \cdot \frac{1}{K} \tag{11}$$

with

$$K = \frac{[O_3] \cdot k_9}{[O_3] \cdot k_9 + [CH_4] \cdot k_8}. \tag{12}$$

The corresponding Cl-atom concentration is then given by:

$$[Cl] = \frac{d}{dt}[Cl] \cdot \tau_{Cl} \approx \frac{d}{dt}[ClO_y] \cdot \frac{1}{K} \cdot \tau_{Cl} \tag{13}$$

with

$$\tau_{Cl} = \frac{1}{[O_3] \cdot k_9 + [CH_4] \cdot k_8} \tag{14}$$

Introducing the expression for τ_{Cl} in Eq. (13) and using Eq. (10), an estimate of the Cl atom concentration can be obtained:

$$[Cl] = \frac{\frac{d}{dt}[ClO_y]}{[O_3] \cdot k_9} \approx \frac{[ClO_y]}{\tau_0 \cdot [O_3] \cdot k_9} \tag{15}$$

Based on this the CH_4-lifetime in the plume can be derived:

$$\tau_{CH_4} \approx \frac{1}{[Cl] \cdot k_8} \approx \frac{\tau_0 \cdot [O_3] \cdot k_9}{[ClO_y] \cdot k_8}. \tag{16}$$

OCIO and BrO observations in the volcanic plume of Mt. Etna

Gliß et al.

Title Page

Abstract | Introduction

Conclusions | References

Tables | Figures

◀ | ▶

◀ | ▶

Back | Close

Full Screen / Esc

Printer-friendly Version

Interactive Discussion

Note that τ_0 denotes the formation time of OCIO as introduced in Sect. 3.1.3 whereas τ_{CH_4} corresponds to the methane lifetime in the plume.

For the estimation of ClO_y, we determined mean ClO and OCIO concentrations from our retrieval considering only plume ages between 120 and 240 s (see also Sect. 3.1.5). We retrieved values of $\overline{ClO} = 2.0 \times 10^9\,cm^{-3}$ and $\overline{OCIO} = 3.7 \times 10^9\,cm^{-3}$, respectively and hence $\overline{ClO_y} = 5.7 \times 10^9\,cm^{-3}$. Based on our findings discussed in Sect. 3.1.3 (e.g. Fig. 9) we estimated the ClO_y formation time at $\tau_0 = 142$ s.

The typical tropospheric O_3-background should be around 60–80 ppb for this region and altitude (Kalabokas et al., 2013). Since the effective expected CH_4-lifetime in the plume is directly proportional to the prevailing O_3-concentration (Eq. 16), we determined [Cl] and τ_{CH_4} as a function of the O_3-concentration (assuming O_3 mixing ratios between 1–40 ppb) in order to account for possibly depleted ozone in the plume (e.g. von Glasow, 2010). The corresponding Cl-atom concentrations in the plume were found to be $5.1 \times 10^6\,cm^{-3}$ (at 40 ppb O_3), $2.1 \times 10^7\,cm^{-3}$ (at 10 ppb O_3) and $2.1 \times 10^8\,cm^{-3}$ (at 1 ppb O_3). This leads to CH_4-lifetimes of 4.9×10^4 s (14 h at 1 ppb O_3), 5.6 days at 10 ppb O_3 and 23 days at 40 ppb O_3.

These lifetimes for the conditions in September 2012 at Mt. Etna are more than two orders of magnitude shorter than the average atmospheric lifetime of CH_4. Nevertheless, if O_3 is not strongly depleted in the plume, CH_4 destruction by Cl-atoms will probably not lead to detectable loss of CH_4 since it is unlikely that the Cl-levels derived from our measurements prevail for more than very few hours (i.a. due to plume dilution). During this time less than 1 % of the CH_4 in the plume will be destroyed, assuming that the mean abundance of O_3 in the plume exceeds 10 ppb. However, in regions of really low O_3 concentrations (i.e. possibly in the plume centre, von Glasow, 2010) a significant loss of CH_4 could be present but the effect on the surrounding atmosphere would probably still be negligible since the effective volume of this potential methane depleting environment would be very small. However, CH_4 depletion may become detectable for stronger emissions of chlorine combined with conditions more favourable to Cl-activation.

Title Page

Abstract	Introduction
Conclusions	References
Tables	Figures

|◀ | ▶|

◀ | ▶

Back | Close

Full Screen / Esc

Printer-friendly Version

Interactive Discussion

3.2 Results for IO, OIO and OBrO

We investigated the presence of IO (UV), OIO and OBrO (both VIS) employing the extended spectral range due to the second spectrograph. We did not detect any of these species in the spectra of this field campaign and therefore only present the corresponding DOAS detection limits (see tab. 4).

The mixing ratios r_i (column three) were determined as suggested in Sect. 2.5. We give both the detection limits for plume ages smaller and larger than three minutes since it appears reasonable to assume, that these species – if abundant in the plume – show similar formation processes as observed in case of BrO and OClO (for details see 3.1.3). We used a fixed fit correction factor U (see Sect. 2.4.1) of $U = 5$ for OBrO and OIO and $U = 4$ for IO respectively. These – comparatively large – correction factors were chosen in order to have a rather conservative estimate of the detection limits.

4 Conclusions

We provide a dataset of simultaneous OClO and BrO distributions measured in the volcanic plume of Mt. Etna using the MAX-DOAS method. Ratios of the retrieved BrO and OClO-SCDs with the corresponding SO_2-SCDs were studied (i.e. BrO/SO_2 and OClO/SO_2) in order to separate the chemical evolution of the observed halogen species from plume dilution effects in the SCDs (SO_2 was treated as a passive plume-proxy).

Observation of the BrO and OClO formation in the young plume

Both the BrO/SO_2 and the OClO/SO_2-ratio showed a strong increase in the first three minutes after release and a levelling off later on. The increasing ratios were associated to the formation of BrO and OClO in the young plume from the emitted hydrogen halides (HBr, HCl). For these measurements we used an improved MAX-DOAS scanning algorithm performed along the plume propagation axis. The increase

could be observed in six individual scans on two different measurement days. It could furthermore be confirmed in an additional statistical analysis of our retrieval in the young plume. Using these results we estimated the formation duration (τ_0) of the measured halogens in the young plume (i.e. the time scale until the respective X_mO_n/SO_2-ratio levels off reaching a steady state value). The statistical approach revealed a mean formation time of $\tau_0 = 142$ s both for BrO and OClO. The individual scans rather indicated some variations in the absolute value of τ_0 (probably due to uncertainties in the plume age determination). The corresponding values ranged between $\tau_0 = 24$–154 s (BrO) and $\tau_0 = 85$–226 s (OClO). Hence, the direct observations rather suggest a slightly longer (up to 73 s) formation time for OClO compared to BrO. Mean abundances for the stabilised plume age regime (i.e. $\tau < \tau_0$) were 3.17×10^{-5} for OClO/SO$_2$, 1.55×10^{-4} for BrO/SO$_2$ and 0.16 for OClO/BrO.

Increased BrO/SO$_2$ and OClO/SO$_2$-ratios at the edges

Scans performed perpendicular to the plume propagation axis showed enhanced BrO/SO$_2$-ratios at the plume edges compared to the plume-centre (in 76 % of all analysed scans). We derived mean centre-to-edge enhancements between 30–37 % for BrO/SO$_2$. Furthermore, we found indications of increased OClO/SO$_2$-ratios at the edges with enhancements between 10–250 %. Unfortunately, this trend could not be confirmed with certainty since suitable data for the cross sectional analysis of OClO was strongly limited especially in the plume edge regime.

Correction for stratospheric BrO signals

We implemented a correction for stratospheric BrO signals (dSCDs) in our retrieval. These signals arise with increasing differences in the solar zenith angle (SZA) between plume spectrum and Fraunhofer reference spectrum. The stratospheric BrO

load (VCD) was estimated using own measurements and published literature values. Based on this, we corrected the retrieved BrO-SCDs by their stratospheric BrO-amount (dSCD). In most cases (85 %) the impact on our retrieval was comparatively small (< 5 %). Only in ∼ 8 % of the measurements (i.e. solely performed at large SZAs) the additional stratospheric signal affected our plume BrO-retrieval significantly.

Observation of the photochemical formation of BrO and OClO in the early morning

We were furthermore able to observe an increase of the BrO/SO_2-ratio with time just after sunrise and a levelling off later on. The corresponding measurement was performed with the telescope pointing to a single spot in the plume. This observation constitutes a further indication that photochemistry is an important parameter in the formation of BrO (i.e. the "bromine-explosion"). Observing this trend was only possible due to the implemented correction for stratospheric BrO signals (previous paragraph). The corresponding $OClO/SO_2$-ratio also showed strong indications of an increasing trend levelling off approximately 40 min later than BrO. Our stated hypothesis for this delay was that it could indicate a lack of gaseous chlorine (and hence ClO) during the time shortly after sunrise (since the major part of OClO is probably formed via the "BrO + ClO"-reaction).

In summary these observations, namely

 i. the BrO and OClO increase in the first minutes downwind,

 ii. the elevated values at the plume edges,

 iii. and the photochemical formation of BrO and OClO in the early morning

Title Page

Abstract | Introduction

Conclusions | References

Tables | Figures

◄ | ►

◄ | ►

Back | Close

Full Screen / Esc

Printer-friendly Version

Interactive Discussion

confirm the current understanding of the chemistry of reactive halogens in volcanic plumes namely the "bromine explosion" (BrO formation) and furthermore the gas-phase formation of OClO ("BrO + ClO"-reaction).

Upper limits for IO, OIO and OBrO in the plume

5   We furthermore analysed the data for spectral signatures of IO, OIO and OBrO but were not able to detect any of the species significantly. Our detection limits for IO/SO$_2$, OIO/SO$_2$ and OBrO/SO$_2$ are 1.8×10^{-6}, 2.0×10^{-5} and 1.1×10^{-5} (plume age $\tau <$ 3 min) and 5.2×10^{-6}, 2.8×10^{-5} and 1.8×10^{-5} ($\tau >$ 3 min) respectively.

Estimation of ClO, OClO and BrO concentrations in the plume

10   We estimated ClO abundances in the plume using our retrieved BrO and OClO-SCDs. The ClO mixing ratios were at levels of 70–235 ppt and could be determined up to plume ages of six minutes. We furthermore determined mean concentrations of OClO and BrO from the SCDs by estimating an effective plume diameter from the SO$_2$-profiles. For this estimation, we assumed a circular plume shape and neglected pos-
15   sible effects of radiation transport in and around the plume (e.g. multiple scattering). We retrieved BrO concentrations between 11 ppt and 2.7 ppb covering plume ages up to 17 min. As expected, the concentrations decreased with increasing plume age (due to plume dispersion). The determined OClO concentrations ranged from 36 to 597 ppt and could be determined up to plume ages of six minutes. Mean abundances
20   in the young plume ($\tau <$ 4 min) were estimated to $\overline{ClO}$ = 139 ppt, $\overline{BrO}$ = 1.35 ppb and $\overline{OClO}$ = 300 ppt respectively. A possible decrease of the OClO/ClO-ratio with increasing plume age might have been observed in a single measurement but has to be investigated further since systematic errors in the determination of the OClO (and BrO) concentrations could not be ruled out.

Cl-concentrations and possible depletion of CH₄ in the plume

We estimated abundances of Cl-atoms in the plume using the observed formation times of BrO and OClO in the young plume together with the determined concentrations of ClO and OClO. Depending on the assumed levels of O_3 in the plume Cl-concentrations ranged from 5.1×10^6 cm^{-3} (at 40 ppb O_3) to 2.1×10^8 cm^{-3} (at 1 ppb O_3). Based on this, we addressed a potential depletion of CH_4 in the plume and found CH_4-lifetimes between 23 days (at 40 ppb O_3) and 14 h (at 1 ppb O_3). Compared to the atmospheric lifetime of CH_4 ($\sim$ 9 a) these lifetimes are relatively short. However, the effect on the CH_4-budget in the plume should be relatively small, since the prevailing Cl-concentrations decrease rapidly (due to plume dispersion). In fact our results indicate that it would be difficult to observe a reduction of the CH_4-levels inside the plume.

References

Beirle, S., Hörmann, C., Penning de Vries, M., Dörner, S., Kern, C., and Wagner, T.: Estimating the volcanic emission rate and atmospheric lifetime of SO_2 from space: a case study for

Title Page

Abstract | Introduction

Conclusions | References

Tables | Figures

◄ | ►

◄ | ►

Back | Close

Full Screen / Esc

Printer-friendly Version

Interactive Discussion

Kīlauea volcano, Hawai'i, Atmos. Chem. Phys., 14, 8309–8322, doi:10.5194/acp-14-8309-2014, 2014. 25236

Birks, J. W., Shoemaker, B., Leck, T. J., Borders, R. A., and Hart, L. J.: Studies of reactions of importance in the stratosphere, II. Reactions involving chlorine nitrate and chlorine dioxide, J. Chem. Phys., 66, 4591–4599, doi:10.1063/1.433716, available at: http://scitation.aip.org/content/aip/journal/jcp/66/10/10.1063/1.433716, 1977. 25231

Bobrowski, N. and Giuffrida, G.: Bromine monoxide/sulphur dioxide ratios in relation to volcanological observations at Mt. Etna 2006–2009, Solid Earth, 3, 433–445, doi:10.5194/se-3-433-2012, 2012. 25217, 25238

Bobrowski, N. and Platt, U.: SO_2/BrO ratios studied in five volcanic plumes, J. Volcanol. Geoth. Res., 166, 147–160, doi:10.1016/j.jvolgeores.2007.07.003, 2007. 25236

Bobrowski, N., Honninger, G., Galle, B., and Platt, U.: Detection of bromine monoxide in a volcanic plume, NATURE, 423, 273–276, doi:10.1038/nature01625, 2003. 25216, 25229, 25236

Bobrowski, N., von Glasow, R., Aiuppa, A., Inguaggiato, S., Louban, I., Ibrahim, O. W., and Platt, U.: Reactive halogen chemistry in volcanic plumes, J. Geophys. Res.-Atmos., 112, D06311, doi:10.1029/2006JD007206, 2007. 25217, 25219, 25220, 25236, 25238, 25239, 25242

Bobrowski, N., Kern, C., Platt, U., Hörmann, C., and Wagner, T.: Novel SO_2 spectral evaluation scheme using the 360–390 nm wavelength range, Atmos. Meas. Tech., 3, 879–891, doi:10.5194/amt-3-879-2010, 2010. 25228

Bogumil, K., Orphal, J., Homann, T., Voigt, S., Spietz, P., Fleischmann, O., Vogel, A., Hartmann, M., Kromminga, H., Bovensmann, H., Frerick, J., and Burrows, J.: Measurements of molecular absorption spectra with the SCIAMACHY pre-flight model: instrument characterization and reference data for atmospheric remote-sensing in the 230–2380 nm region, J. Photoch. Photobio. A, 157, 167–184, doi:10.1016/S1010-6030(03)00062-5, 2003. 25262

Burrows, J., Richter, A., Dehn, A., Deters, B., Himmelmann, S., and Orphal, J.: Atmospheric remote-sensing reference data from GOME-2, temperature-dependent absorption cross sections of O–3 in the 231–794 nm range, J. Quant. Spectrosc. RA, 61, 509–517, doi:10.1016/S0022-4073(98)00037-5, 1999. 25262

Carroll, M. R. and Holloway, J. R.: Volatiles in magmas, Mineralogical Society of America, http://www.minsocam.org/msa/rim/Rim30.html (last access: 29 September 2014), ISBN 0-939950-36-7ISBN13 978-0-939950-36-2, 517 pp., 1994. 25215, 25216

OCIO and BrO observations in the volcanic plume of Mt. Etna

Gliß et al.

Title Page

Abstract	Introduction
Conclusions	References
Tables	Figures

|◀ | ▶|

◀ | ▶

Back | Close

Full Screen / Esc

Printer-friendly Version

Interactive Discussion

Chance, K. and Kurucz, R.: An improved high-resolution solar reference spectrum for earth's atmosphere measurements in the ultraviolet, visible, and near infrared, J. Quant. Spectrosc. RA, 111, 1289–1295, doi:10.1016/j.jqsrt.2010.01.036, 2010. 25224

Donovan, A., Tsanev, V., Oppenheimer, C., and Edmonds, M.: Reactive halogens (BrO and OClO) detected in the plume of Soufrière Hills Volcano during an eruption hiatus, Geochem. Geophy. Geosy., 15, 3346–3363, doi:10.1002/2014GC005419, 2014. 25216, 25219, 25226

Fickert, S., Adams, J. W., and Crowley, J. N.: Activation of Br_2 and BrCl via uptake of HOBr onto aqueous salt solutions, J. Geophys. Res.-Atmos., 104, 23719–23727, doi:10.1029/1999JD900359, 1999. 25218

Fleischmann, O. and Burrows, J. P.: UV/VIS absorption spectrum of OBrO, availabe at: http://satellite.mpic.de/spectral_atlas/cross_sections/Halogen%20oxides/Br%20oxides/OBrO_FleischmannBurrows%282002%29_298K_384-616nm%285cm-1%29.txt (last access: 25 September 2014), unpublished OBrO cross section, private communication, University of Bremen, 2002. 25262

Francis, P., Maciejewski, A., Oppenheimer, C., Chaffin, C., and Caltabiano, T.: SO_2 : HCl ratios in the plumes from Mt. Etna and Vulcano determined by Fourier Transform Spectroscopy, Geophys. Res. Lett., 22, 1717–1720, doi:10.1029/95GL01657, 1995. 25216

General, S., Bobrowski, N., Pöhler, D., Weber, K., Fischer, C., and Platt, U.: Airborne I-DOAS measurements at Mt. Etna: BrO and OClO evolution in the plume, J. Volcanol. Geoth. Res., doi:10.1016/j.jvolgeores.2014.05.012, in press, 2014. 25219, 25220, 25238, 25239

Gerlach, T.: Volcanic sources of tropospheric ozone-depleting trace gases, Geochem. Geophy. Geosy., 5, Q09007, doi:10.1029/2004GC000747, 2004. 25216, 25217

Greenblatt, G. D., Orlando, J. J., Burkholder, J. B., and Ravishankara, A. R.: Absorption measurements of oxygen between 330 and 1140 nm, J. Geophys. Res.-Atmos., 95, 18577–18582, doi:10.1029/JD095iD11p18577, 1990. 25262

Hermans, C., A. C., V., Fally, S., Carleer, M., Colin, R., Coquart, B., Jenouvrier, A., and Merienne, M.- F.: Absorption cross-section of the collision-induced bands of oxygen from the UV to the NIR, Proceedings of the NATO Advanced Research Workshop, Weakly Interacting Molecular Pairs: Unconventional Absorbers of Radiation in the Atmosphere, France, 24 April–2 May 2002, NATO Science Series IV Earth and Environmental Sciences, 27, 193–202, available at: http://www.aeronomie.be/spectrolab/o2.htm, 2003. 25262

Title Page

Abstract | Introduction

Conclusions | References

Tables | Figures

|◄ | ►|

◄ | ►

Back | Close

Full Screen / Esc

Printer-friendly Version

Interactive Discussion

Hermans, C., Vandaele, A., and Fally, S.: Fourier transform measurements of SO_2 absorption cross sections: I. Temperature dependence in the 24 000–29 000 cm^{-1} (345–420 nm) region, J. Quant. Spectrosc. Ra., 110, 756–765, doi:10.1016/j.jqsrt.2009.01.031, 2009. 25262

Hönninger, G., von Friedeburg, C., and Platt, U.: Multi axis differential optical absorption spectroscopy (MAX-DOAS), Atmos. Chem. Phys., 4, 231–254, doi:10.5194/acp-4-231-2004, 2004. 25215, 25234

Hörmann, C., Sihler, H., Bobrowski, N., Beirle, S., Penning de Vries, M., Platt, U., and Wagner, T.: Systematic investigation of bromine monoxide in volcanic plumes from space by using the GOME-2 instrument, Atmos. Chem. Phys., 13, 4749-4781, doi:10.5194/acp-13-4749-2013, 2013. 25228

Kalabokas, P. D., Cammas, J.- P., Thouret, V., Volz-Thomas, A., Boulanger, D., and Repapis, C. C.: Examination of the atmospheric conditions associated with high and low summer ozone levels in the lower troposphere over the eastern Mediterranean, Atmos. Chem. Phys., 13, 10339-10352, doi:10.5194/acp-13-10339-2013, 2013. 25249

Kern, C., Sihler, H., Vogel, L., Rivera, C., Herrera, M., and Platt, U.: Halogen oxide measurements at Masaya Volcano, Nicaragua using active long path differential optical absorption spectroscopy, B. Volcanol., 71, 659–670, doi:10.1007/s00445-008-0252-8, 2009. 25220, 25230, 25236, 25244

Kern, C., Deutschmann, T., Vogel, L., Woehrbach, M., Wagner, T., and Platt, U.: Radiative transfer corrections for accurate spectroscopic measurements of volcanic gas emissions, B. Volcanol., 72, 233–247, doi:10.1007/s00445-009-0313-7, 2010. 25228, 25230

Kraus, S.: DOASIS: A framework design for DOAS, Shaker, http://books.google.no/books?id=GFF5AAAACAAJ (last access: 25 September 2014), 2006. 25223, 25224, 25225

Lee, C., Kim, Y. J., Tanimoto, H., Bobrowski, N., Platt, U., Mori, T., Yamamoto, K., and Hong, C. S.: High ClO and ozone depletion observed in the plume of Sakurajima volcano, Japan, Geophys. Res. Lett., 32, L21809, doi:10.1029/2005GL023785, 2005. 25219, 25229

Lee, C., Martin, R. V., van Donkelaar, A., Lee, H., Dickerson, R. R., Hains, J. C., Krotkov, N., Richter, A., Vinnikov, K., and Schwab, J. J.: SO_2 emissions and lifetimes: estimates from inverse modeling using in situ and global, space-based (SCIAMACHY and OMI) observations, J. Geophys. Res.-Atmos., 116, D06304, doi:10.1029/2010JD014758, 2011. 25236

Lehrer, E., Wagenbach, D., and Platt, U.: Aerosol chemical composition during tropospheric ozone depletion at Ny Alesund/Svalbard, Tellus B, 49, 486–495, doi:10.1034/j.1600-0889.49.issue5.5.x, 1997. 25217

OCIO and BrO observations in the volcanic plume of Mt. Etna

Gliß et al.

Title Page

Abstract | Introduction

Conclusions | References

Tables | Figures

◄ | ►

◄ | ►

Back | Close

Full Screen / Esc

Printer-friendly Version

Interactive Discussion

Louban, I., Bobrowski, N., Rouwet, D., Inguaggiato, S., and Platt, U.: Imaging DOAS for vol-canological applications, B. Volcanol., 71, 753–765, doi:10.1007/s00445-008-0262-6, 2009. 25239

Martin, R., Mather, T., and Pyle, D.: High-temperature mixtures of magmatic and atmospheric gases, Geochem. Geophy. Geosy., 7, Q04006, doi:10.1029/2005GC001186, 2006. 25217

Martin, R. S., Mather, T. A., Pyle, D. M., Power, M., Allen, A. G., Aiuppa, A., Horwell, C. J., and Ward, E. P. W.: Composition-resolved size distributions of volcanic aerosols in the Mt. Etna plumes, J. Geophys. Res.-Atmos., 113, D17211, doi:10.1029/2007JD009648, 2008. 25218

Mayer, B. and Kylling, A.: Technical note: The libRadtran software package for radiative trans-fer calculations – description and examples of use, Atmos. Chem. Phys., 5, 1855-1877, doi:10.5194/acp-5-1855-2005, 2005. 25230

McGonigle, A. J. S., Delmelle, P., Oppenheimer, C., Tsanev, V. I., Delfosse, T., Williams-Jones, G., Horton, K., and Mather, T. A.: SO_2 depletion in tropospheric volcanic plumes, Geophys. Res. Lett., 31, L13201, doi:10.1029/2004GL019990, 2004. 25236

Meller, R. and Moortgat, G.: Temperature dependence of the absorption cross sections of formaldehyde between 223 and 323 K in the wavelength range 225–375 nm, J. Geophys. Res.-Atmos., 105, 7089–7101, doi:10.1029/1999JD901074, 2000. 25262

Oppenheimer, C., Tsanev, V. I., Braban, C. F., Cox, R. A., Adams, J. W., Aiuppa, A., Bo-browski, N., Delmelle, P., Barclay, J., and McGonigle, A. J. S.: BrO formation in volcanic plumes, Geochim. Cosmochim. Ac., 70, 2935–2941, doi:10.1016/j.gca.2006.04.001, 2006. 25217

Platt, U. and Stutz, J.: Differential Optical Absorption Spectroscopy: Principles and Application, Springer, doi:10.1007/978-3-540-75776-4, 2008. 25223, 25224

Pyle, D. and Mather, T.: Halogens in igneous processes and their fluxes to the at-mosphere and oceans from volcanic activity: a review, Chem. Geol., 263, 110–121, doi:10.1016/j.chemgeo.2008.11.013, 2009. 25216, 25220

Roberts, T., Braban, C., Martin, R., Oppenheimer, C., Adams, J., Cox, R., Jones, R., and Grif-fiths, P.: Modelling reactive halogen formation and ozone depletion in volcanic plumes, Chem. Geol., 263, 151–163, doi:10.1029/JD095iD11p18577, 2009. 25217

Robock, A.: Volcanic eruptions and climate, Rev. Geophys., 38, 191–219, doi:10.1029/1998RG000054, 2000. 25216

Sander, S. P., Friedl, R. R., Golden, D. M., Kurylo, M. J., Moortgat, G. K., Keller-Rudeck, H., Wine, P. H., Ravishankara, A. R., Kolb, C. E., Molina, M. J., Finlaysson-Pitts, B. J., Huie, R. E.,

Title Page

Abstract | Introduction

Conclusions | References

Tables | Figures

|◄ | ►|

◄ | ►

Back | Close

Full Screen / Esc

Printer-friendly Version

Interactive Discussion

and Orkin, R. L.: Chemical Kinetics and Photochemical Data for Use in Atmospheric Studies, Tech. Rep. Evaluation Number 15, JPL Publication, 06–2, Jet Propolsion Laboratory, NASA, available at: http://jpldataeval.jpl.nasa.gov/, 2006. 25219, 25247

Schofield, R., Kreher, K., Connor, B. J., Johnston, P. V., Thomas, A., Shooter, D., Chipperfield, M. P., Rodgers, C. D., and Mount, G. H.: Retrieved tropospheric and stratospheric BrO columns over Lauder, New Zealand, J. Geophys. Res.-Atmos., 109, D14304, doi:10.1029/2003JD004463, 2004. 25234, 25235

Sinnhuber, B.- M., Rozanov, A., Sheode, N., Afe, O. T., Richter, A., Sinnhuber, M., Wittrock, F., Burrows, J. P., Stiller, G. P., von Clarmann, T., and Linden, A.: Global observations of stratospheric bromine monoxide from SCIAMACHY, Geophys. Res. Lett., 32, L20810, doi:10.1029/2005GL023839, 2005. 25234, 25235

Spietz, P., Martín, J. C. G., and Burrows, J. P.: Spectroscopic studies of the I2/O3 photochemistry: Part 2. Improved spectra of iodine oxides and analysis of the {IO} absorption spectrum, J. Photoch. Photobio. A, 176, 50–67, doi:10.1016/j.jphotochem.2005.08.023, 2005. 25262

Stutz, J. and Platt, U.: Numerical analysis and estimation of the statistical error of differential optical absorption spectroscopy measurements with least-squares methods, Appl. Opt., 35, 6041–6053, doi:10.1364/AO.35.006041, 1996. 25225, 25226, 25227

Theys, N., De Smedt, I., Van Roozendael, M., Froidevaux, L., Clarisse, L., and Hendrick, F.: First satellite detection of volcanic OClO after the eruption of Puyehue-Cordón Caulle, Geophys. Res. Lett., 41, 667–672, doi:10.1002/2013GL058416, 2014. 25219, 25220

Vogel, L.: Volcanic plumes: Evaluation of spectroscopic measurements, early detection and bromine chemistry, Ph. D. thesis, Combined Faculties for the Natural Sciences and for Mathematics, Ruperto Carola University of Heidelberg, Germany, available at: http://archiv.ub.uni-heidelberg.de/volltextserver/13219/, 2011. 25228

Voigt, S., Orphal, J., and Burrows, J.: The temperature and pressure dependence of the absorption cross-sections of NO_2 in the 250–800 nm region measured by Fourier-transform spectroscopy, J. Photoch. Photobio. A, 149, 1–7, doi:10.1016/S1010-6030(01)00650-5, 2002. 25262

von Glasow, R.: Atmospheric chemistry in volcanic plumes, P. Natl. Acad. Sci. USA, 107, 6594–6599, doi:10.1073/pnas.0913164107, 2010. 25220, 25249

von Glasow, R., Bobrowski, N., and Kern, C.: The effects of volcanic eruptions on atmospheric chemistry, Chem. Geol., 263, 131–142, doi:10.1016/j.chemgeo.2008.08.020, 2009. 25218

Title Page

Abstract | Introduction

Conclusions | References

Tables | Figures

◄◄ | ►►

◄ | ►

Back | Close

Full Screen / Esc

Printer-friendly Version

Interactive Discussion

Wagner, T., Beirle, S., and Deutschmann, T.: Three-dimensional simulation of the Ring effect in observations of scattered sun light using Monte Carlo radiative transfer models, Atmos. Meas. Tech., 2, 113-124, doi:10.5194/amt-2-113-2009, 2009. 25224

Wennberg, P.: Atmospheric chemistry: bromine explosion, Nature, 397, 299–301, doi:10.1038/16805, 1999. 25217

Wilmouth, D. M., Hanisco, T. F., Donahue, N. M., and Anderson, J. G.: Fourier transform ultraviolet spectroscopy of the $A^2\Pi_{(3/2)} \leftarrow X^2\Pi_{(3/2)}$ transition of BrO, J. Phys. Chem. A, 103, 8935–8945, doi:10.1021/jp991651o, available at: http://pubs.acs.org/doi/abs/10.1021/jp991651o, 1999. 25262

Wittmer, J., Bobrowski, N., Liotta, M., Giuffrida, G., Calabrese, S., and Platt, U.: Active alkaline traps to determine acidic-gas ratios in volcanic plumes: Sampling techniques and analytical methods, Geochem. Geophy. Geosy., 15, 2797–2820, doi:10.1002/2013GC005133, 2014. 25218

Table 1. Overview of the evaluation ranges of the several trace gases which were evaluated in the scope of this study. Column three lists the species which were additionally included into the respective fitting routine. SO_2, BrO, OClO and IO were evaluated with the UV-spectrograph of the instrument, OBrO and OIO with the VIS-spectrograph respectively. In case of O_4 two different literature cross sections were used (labelled with (1) and (2), for details see table 2). Note: the two Ring spectra ($R, R4$) and the FRS (see Sect. 2.4) are not listed in this table since they were included in each fitting-routine.

Species	$\Delta\lambda$ [nm]	Additional species
SO_2^{lwr}	314.8–326.8	O_3
SO_2^{uwr}	349.8–372.8	BrO, OClO, O_3, O_4, NO_2, CH_2O
BrO and OClO^{lwr}	330.6–356.3	SO_2, O_3, $^{(1)}O_4$, NO_2, CH_2O
OClO^{uwr}	363.6–391.3	SO_2, O_3, $^{(1)}O_4$, NO_2
IO	416.6–441.3	H_2O, NO_2, $^{(2)}O_4$
OBrO	493.2–537.3	H_2O, NO_2, O_3, $^{(2)}O_4$
OIO	547.2–566.5	H_2O, NO_2, O_3, $^{(2)}O_4$, OBrO

Table 2. Literature cross sections which were used in this study. Note that two different cross sections were used for O_4.

Trace gas	Literature cross section
SO_2	Hermans et al. (2009) (298 K)
BrO	Wilmouth et al. (1999) (298 K)
OBrO	Fleischmann and Burrows (2002) (298 K)
OClO	Bogumil et al. (2003) (293 K)
O_3	Burrows et al. (1999) (221 K)
$^{(1)}O_4$	Hermans et al. (2003)
$^{(2)}O_4$	Greenblatt et al. (1990) (vacuum, modified by J. Burkholder)
IO	Spietz et al. (2005) (298 K)
OIO	Spietz et al. (2005) (298 K)
NO_2	Voigt et al. (2002) (293 K)
H_2O	Hitran database 2009 (273 K, 1020 hPa, 300–600 nm)
CH_2O	Meller and Moortgat (2000) (298 K)

Table 3. Formation times (τ_0) of BrO and OClO.

#	Date	Time [UTC]	Plume age range		Stabilisation τ_0 [s]		
			Min [s]	Max [s]	BrO/SO$_2$	OClO/SO$_2$	Δ [s]
1	11 Sept 2012	12:08–12:23	0	199	123	123	0
2	11 Sept 2012	12:56–13:18	0	226	154	176–226	22–72
3	12 Sept 2012	08:15–08:36	124	205	$\leq$ 124	131	$\geq$ 7
4	12 Sept 2012	08:49–09:09	124	205	$\leq$ 124	131–184	$\geq$ 7–60
5	12 Sept 2012	10:25–10:49	24	222	24–36	85–97	49–73
6	12 Sept 2012	11:02–11:35	24	222	48	85	37
7	Statistical analysis		0	250	142	142	0

Table 4. Upper limits of IO, OIO and OBrO. The individual values (SCD, X_mO_n/SO_2, r_i) for each species do not correspond to the same plume spectrum but were determined individually.

Species	SCD [cm^{-2}]	X_mO_n/SO_2	r_i [ppt]
Plume age $\tau < 3\,\mathrm{min}$			
IO	8.6×10^{12}	1.8×10^{-6}	29
OIO	7.8×10^{13}	2.0×10^{-5}	294
OBrO	4.5×10^{13}	1.1×10^{-5}	164
Plume age $\tau > 3\,\mathrm{min}$			
IO	7.6×10^{12}	5.2×10^{-6}	4
OIO	7.5×10^{13}	2.8×10^{-5}	25
OBrO	3.6×10^{13}	1.8×10^{-5}	12

Table A1. Cross section analysis of the X_mO_n/SO_2-ratio for BrO (Subtable 1) and OClO (Subtable 2). Only plume cross section scans (see Sect. 2.3) showing a significant range of SO_2-SCDs were analysed (the range of retrieved SO_2-SCDs for each scan is given in columns 6 and 7, SO_2-SCD). The plume was separated into an edge range and centre range by its SO_2-profile: spectra with SO_2-SCDs smaller than 50 % of the maximum SO_2-SCD of the scan were associated to the plume edge, all others (i.e. $SO_2 \geq 1/2 \times SO_{2,max}$) to the plume centre, respectively. The SO_2-threshold for each scan is denoted as SO_2-Lim. For each scan (rows) the mean (percentage) change of the BrO/SO_2 and $OClO/SO_2$-ratios between edge and centre was studied by determining two values (AD and ALL, see Eq. 9). For the determination of the ALL-values, all scan spectra showing a significant SO_2-SCD were included. In case of AD, only spectra showing a significant X_mO_n/SO_2-ratio were included. Furthermore, the mean value and standard deviation ("Mean", "Std") of the averaged ratios in each range (centre/edge) are given as well as the number of spectra used for averaging ("#"). The values given here correspond to those used for the determination of ALL.

					Subtable 1	BrO/SO$_2$-ratio									
					SO$_2$-SCD			SO$_2 \geq$ SO$_2$-Lim			SO$_2 <$ SO$_2$-Lim			Increase	
#	Date (2012)	Start [UTC]	Stop [UTC]	τ [min]	Max	Min [10^{18} cm^{-2}]	Lim	#	Mean$_1$ E-4	Std$_1$ E-4	#	Mean$_2$ E-4	Std$_2$ E-4	AD [%]	ALL [%]
1	11 Sept.	08:49	09:21	1.1	6.47	0.07	3.24	6	1.02	0.16	5	1.60	0.10	49	56
2	11 Sept.	10:55	11:14	1.5	2.22	0.08	1.11	2	1.19	0.08	8	1.19	0.20	9	0
3	11 Sept.	11:17	11:35	0.7	3.96	0.33	1.98	6	0.97	0.14	4	1.01	0.15	4	4
4	12 Sept.	07:00	07:27	3.4	6.35	0.09	3.18	3	1.75	0.06	4	1.73	0.32	−10	−1
5	12 Sept.	09:20	09:47	3.6	4.09	0.17	2.05	6	1.56	0.09	7	1.73	0.20	7	11
6	13 Sept.	07:16	08:02	0.4	8.77	0.57	4.39	6	1.07	0.25	2	1.56	0.31	45	45
7	16 Sept.	08:02	08:38	6.0	1.89	0.17	0.94	5	1.99	0.06	9	2.42	0.45	22	22
8	19 Sept.	08:21	09:01	15.9	0.58	0.19	0.29	11	2.61	0.15	4	2.67	0.12	2	2
9	19 Sept.	09:11	09:14	5.3	0.42	0.12	0.21	2	2.51	0.39	1	2.64			5
10	19 Sept.	09:20	10:02	16.3	0.56	0.09	0.28	8	2.24	0.17	3	2.46	0.26	−3	10

Table A1. continued.

					SO$_2$-SCD			SO$_2 \geq$ SO$_2$-Lim			SO$_2 <$ SO$_2$-Lim			Increase	
					Max Min Lim			#	Mean$_1$	Std$_1$	#	Mean$_2$	Std$_2$	AD	ALL
#	Date (2012)	Start [UTC]	Stop [UTC]	τ [min]	Max	Min	Lim $[10^{18}$ cm$^{-2}]$	#	E-4	E-4	#	E-4	E-4	[%]	[%]

Subtable 1 | BrO/SO$_2$-ratio

#	Date (2012)	Start [UTC]	Stop [UTC]	τ [min]	Max	Min	Lim	#	Mean$_1$ E-4	Std$_1$ E-4	#	Mean$_2$ E-4	Std$_2$ E-4	AD [%]	ALL [%]
11	19 Sept.	10:25	10:42	15.4	0.39	0.09	0.20	7	1.71	0.33	2	0.88	0.33		−49
12	22 Sept.	09:09	09:44	6.4	1.22	0.28	0.61	8	0.59	0.23	2	0.40	0.36		−32
13	22 Sept.	09:58	10:43	7.9	1.27	0.25	0.64	6	0.68	0.10	4	0.61	0.35	34	−10
14	22 Sept.	10:57	11:57	6.9	1.01	0.07	0.50	5	0.78	0.34	3	1.56	0.37	28	101
15	22 Sept.	12:47	13:05	4.7	1.33	0.08	0.67	4	1.14	0.07	2	2.47	1.40	30	116
16	22 Sept.	13:08	13:23	4.8	0.92	0.08	0.46	3	0.85	0.20	2	1.52	0.42	44	79
17	22 Sept.	13:29	13:41	4.9	1.05	0.06	0.52	3	0.95	0.17	1	0.69			−28
18	22 Sept.	13:50	14:06	4.7	1.20	0.03	0.60	2	0.78	0.04	3	1.04	0.14	25	33
19	22 Sept.	14:13	14:22	4.9	1.01	0.35	0.50	1	0.93		1	1.09		17	17
20	23 Sept.	07:30	07:36	6.9	1.69	0.26	0.85	10	1.61	0.16	13	2.18	0.66	28	36
21	23 Sept.	07:48	08:25	7.2	0.72	0.27	0.36	7	1.85	0.18	1	2.34		27	27
22	23 Sept.	08:31	08:35	7.4	1.10	0.26	0.55	13	1.64	0.26	4	1.93	0.49		18
23	23 Sept.	08:49	09:55	6.6	1.04	0.36	0.52	11	0.95	0.12	3	1.18	0.33	61	23
24	23 Sept.	11:09	11:32	7.1	0.95	0.41	0.48	9	0.80	0.12	1	1.15		39	43
25	23 Sept.	11:38	12:02	6.4	0.91	0.43	0.46	9	0.78	0.13	1	1.22		56	56

Subtable 2 | OClO/SO$_2$-ratio

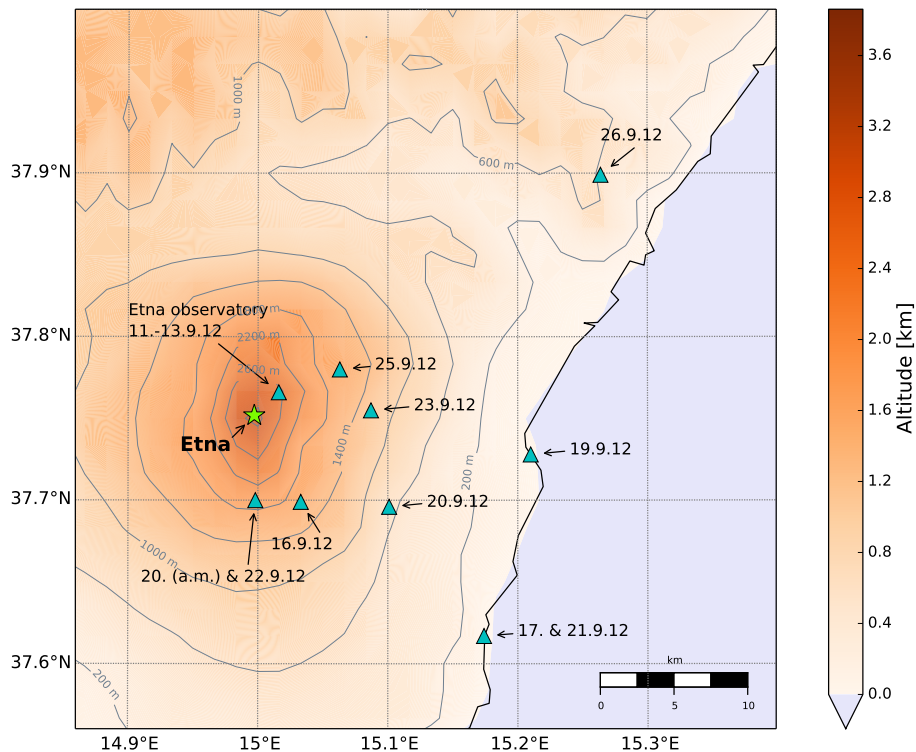| #	Date (2012)	Start [UTC]	Stop [UTC]	τ [min]	Max	Min	Lim	#	Mean$_1$ E-5	Std$_1$ E-5	#	Mean$_2$ E-5	Std$_2$ E-5	AD [%]	ALL [%]
1	11 Sept.	08:49	09:21	1.1	6.47	0.07	3.24	6	1.14	0.37	5	1.02	4.10		−11
2	11 Sept.	10:55	11:14	1.5	2.22	0.08	1.11	2	3.40	0.96	8	2.51	1.91		−26
3	11 Sept.	11:17	11:35	0.7	3.96	0.33	1.98	6	2.21	0.72	4	2.42	0.84		10
4	12 Sept.	07:00	07:27	3.4	6.35	0.09	3.18	3	3.08	0.14	4	15.58	15.12		406
5	12 Sept.	09:20	09:47	3.6	4.09	0.17	2.05	6	2.93	0.36	7	2.31	0.44		−21
6	13 Sept.	07:16	08:02	0.4	8.77	0.57	4.39	6	2.30	0.21	2	4.07	2.37		77
7	16 Sept.	08:02	08:38	6.0	1.89	0.17	0.94	5	4.02	0.44	9	7.13	2.08		77
8	22 Sept.	09:58	10:43	7.9	1.27	0.25	0.64	6	1.61	0.37	4	2.02	1.40		25
9	22 Sept.	12:47	13:05	4.7	1.33	0.08	0.67	4	1.90	0.36	2	6.64	3.59		250

Figure 1. Measurement locations of the Etna campaign, indicated by blue triangles. The summit region with the four active craters (NE, BN, VOR and SE) is indicated by a green star.

Title Page

Abstract   Introduction

Conclusions   References

Tables   Figures

◄   ►|

◄   ►

Back   Close

Full Screen / Esc

Printer-friendly Version

Interactive Discussion

Full Screen / Esc

Printer-friendly Version

Interactive Discussion
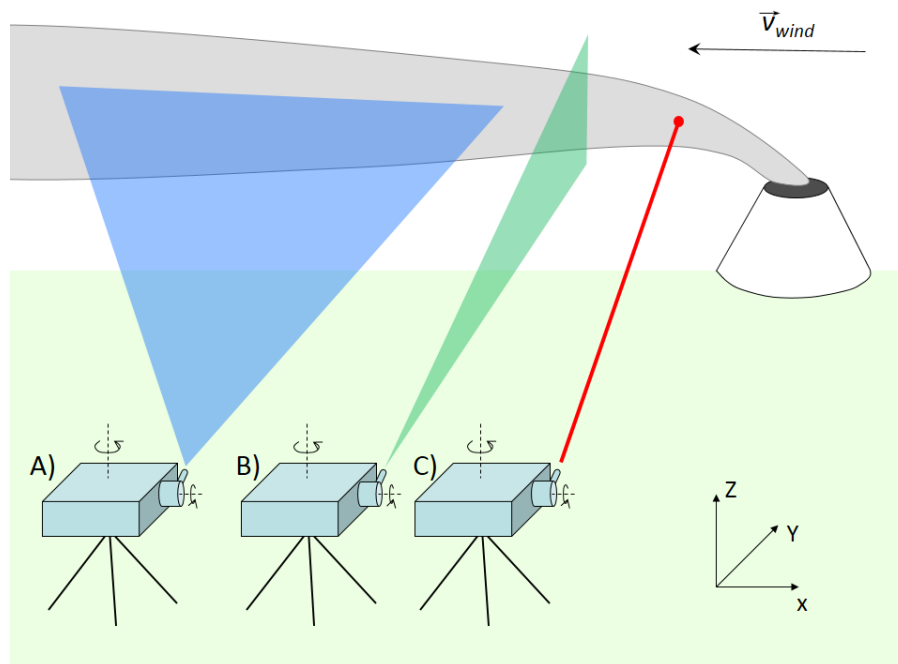
Figure 2. Sketch of the scanning routines: plume evolution scans (**A**, blue) scan stepwise along the plume propagation axis whereas plume cross section scans (**B**, green) scan perpendicular to it. Point measurements (**C**, red) are performed at one spot in the plume without changing the telescopes viewing direction.
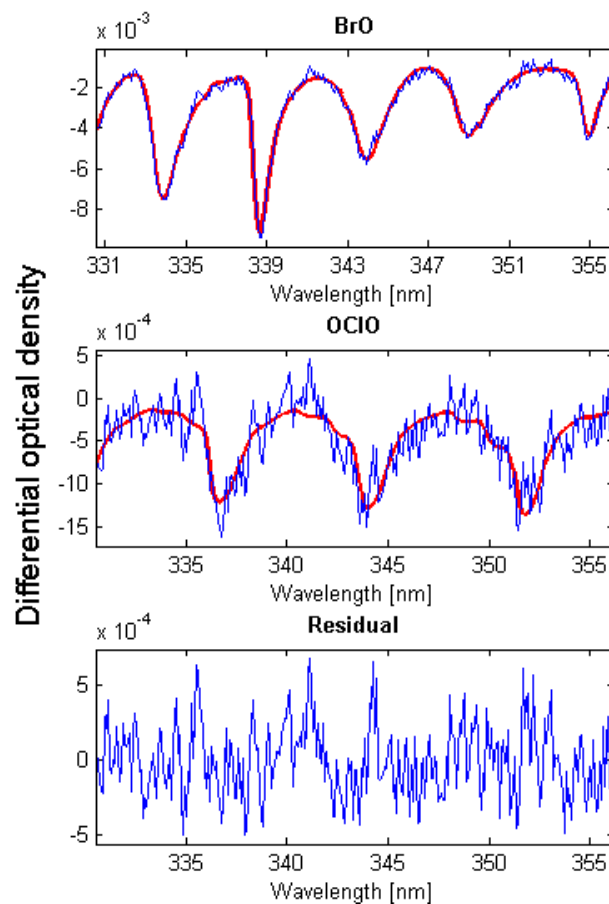
Figure 3. Exemplary fit of BrO ($S_{BrO} = 6.34 \times 10^{14}$ molecules cm^{-2}) and OClO ($S_{OClO} = 1.35 \times 10^{14}$ molecules cm^{-2}) and the corresponding fit-residual.

Discussion Paper | Discussion Paper | Discussion Paper | Discussion Paper |

ACPD

14, 25213–25280, 2014

OClO and BrO observations in the volcanic plume of Mt. Etna

Gliß et al.

Title Page

Abstract | Introduction

Conclusions | References

Tables | Figures

|◄ | ►|

◄ | ►

Back | Close

Full Screen / Esc

Printer-friendly Version

Interactive Discussion
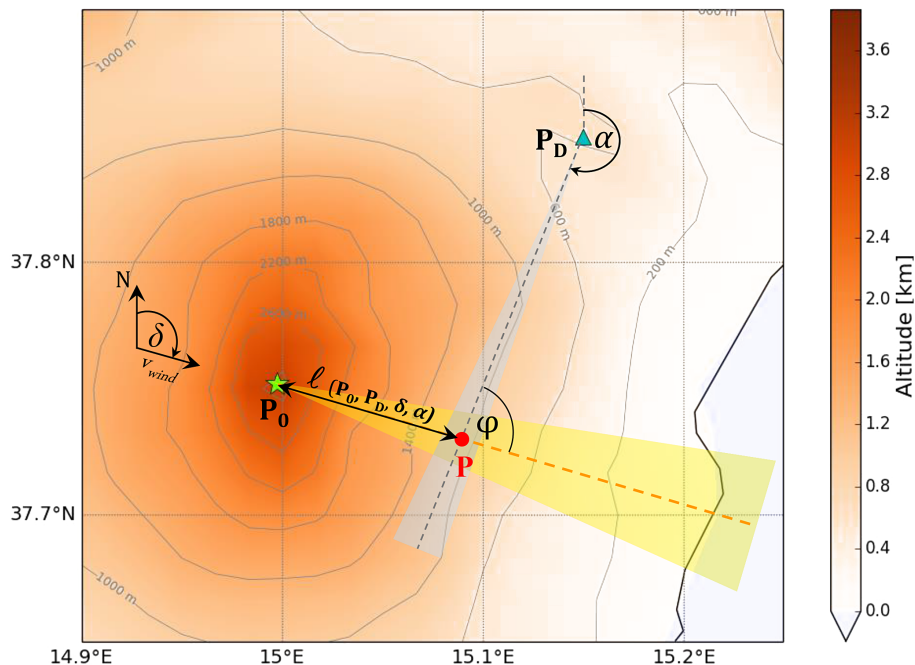
Figure 4. Typical scan geometry for Mt. Etna: the emission source is located at P_0, the DOAS instrument is located at P_D. The intersection point of plume and telescope P is determined from the telescopes viewing direction (α, gray dotted line) and the plume direction (δ, orange dotted line). Typical uncertainties of α and δ are indicated by the gray and yellow shaded area respectively. The plume age τ is determined by dividing $l(P_0, P_D, \delta, \alpha)$ by the wind velocity v_{wind}.

Title Page

Abstract | Introduction

Conclusions | References

Tables | Figures

|◄ | ►|

◄ | ►

Back | Close

Full Screen / Esc

Printer-friendly Version

Interactive Discussion
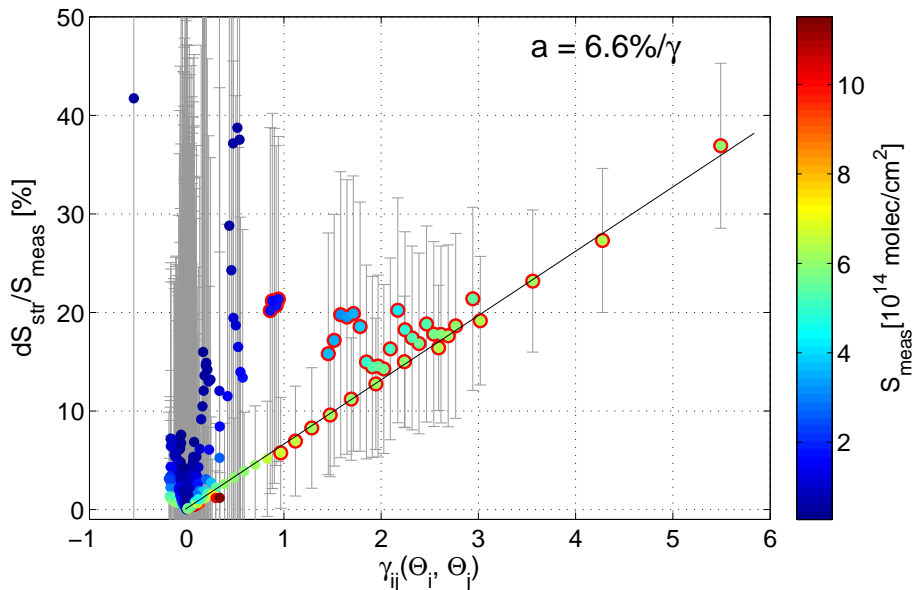
Figure 5. Relative deviation (dS_{str}/S_{meas}) of volcanic BrO from the measured SCDs (S_{meas}, colour coded) due to stratospheric BrO dSCDs. We assumed a vertical stratospheric BrO column of $V_{str,BrO} = 4.0 \times 10^{13}$ molecules cm^{-2}. The results are plotted as a function of ΔSZA represented in the parametrisation $\gamma_{ij}(\Theta_i, \Theta_j)$ (see Eq. 8). We included all spectra from our dataset with significant BrO-SCDs corresponding to the respective detection limit. For 8 % of the data, we observed a significant deviation from the measured SCDs (marked with red circles). Significant deviations were only observed for γ_{ij} values larger than 0.86 and correspond to spectra which were taken before 08:15 LT or after 16:45 LT respectively.

Title Page

Abstract | Introduction

Conclusions | References

Tables | Figures

|◄ | ►|

◄ | ►

Back | Close

Full Screen / Esc

Printer-friendly Version

Interactive Discussion

Title Page

Abstract | Introduction

Conclusions | References

Tables | Figures

|◄ | ►|

◄ | ►
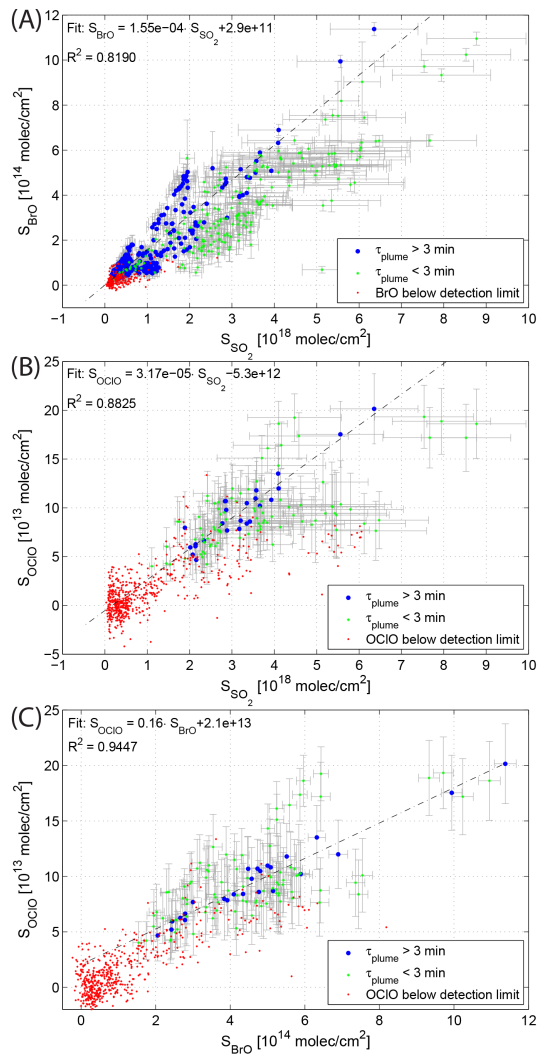
Back | Close

Full Screen / Esc

Printer-friendly Version

Interactive Discussion

Figure 6. Slant column densities of BrO (**A**) and OClO (**B**) as a function of the retrieved SO_2-SCDs and (C) OClO vs. BrO-SCDs. Only spectra showing a significant SO_2-SCD were included. The measurements were subdivided by their plume age τ (i.e. $\tau < 3$ min: green stars, $\tau > 3$ min: blue dots) due to smaller BrO/SO_2 and $OClO/SO_2$-ratios in the young plume (see also Sect. 3.1.3). Measurements below the detection limit of BrO (**A**) and OClO (**B**) are indicated by red dots. We determined mean ratios in the $\tau > 3$ min range (blue dots) by applying a linear fit and found values of $BrO/SO_2 = 1.55 \times 10^{-4}$ and $OClO/SO_2 = 3.17 \times 10^{-5}$ respectively. The OClO/BrO-ratio (**C**) was found to be 0.16 for $\tau > 3$ min and approximately 0.22 in the young plume.
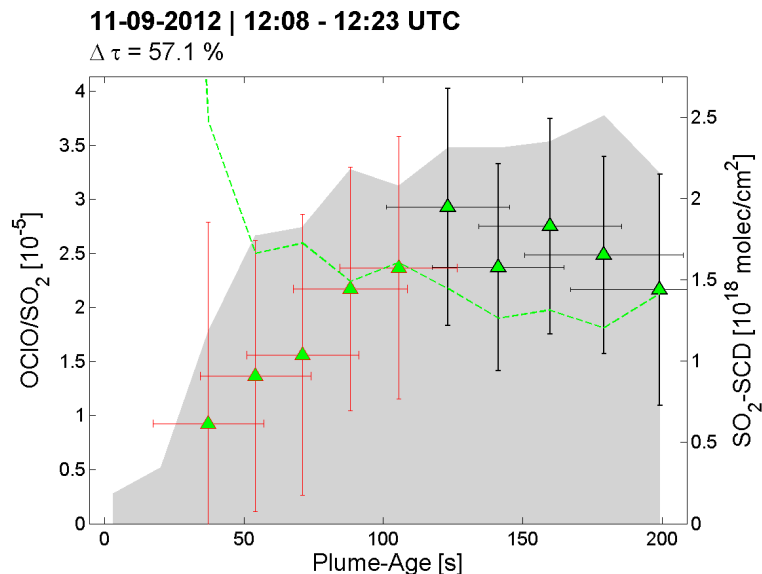
Figure 7. Example of a plume evolution scan of the OClO/SO$_2$ ratio (green triangles) with the corresponding detection limit (green dotted line) as a function of the plume age τ. Red error bars indicate measurements below the detection limit. The SO$_2$-SCDs are plotted as grey shaded areas (right axis). Below $\tau < 50$ s the retrieved SO$_2$-SCDs are comparatively small indicating that these spectra were taken at the plume edge. The OClO/SO$_2$-ratio increases in the young plume ($\tau < 120$ s), starting with data points below the detection limit and reaches a maximum at $\tau = 125$ s. Afterwards it follows a slight decreasing trend (details – especially regarding the error interpretation – are discussed in the text).
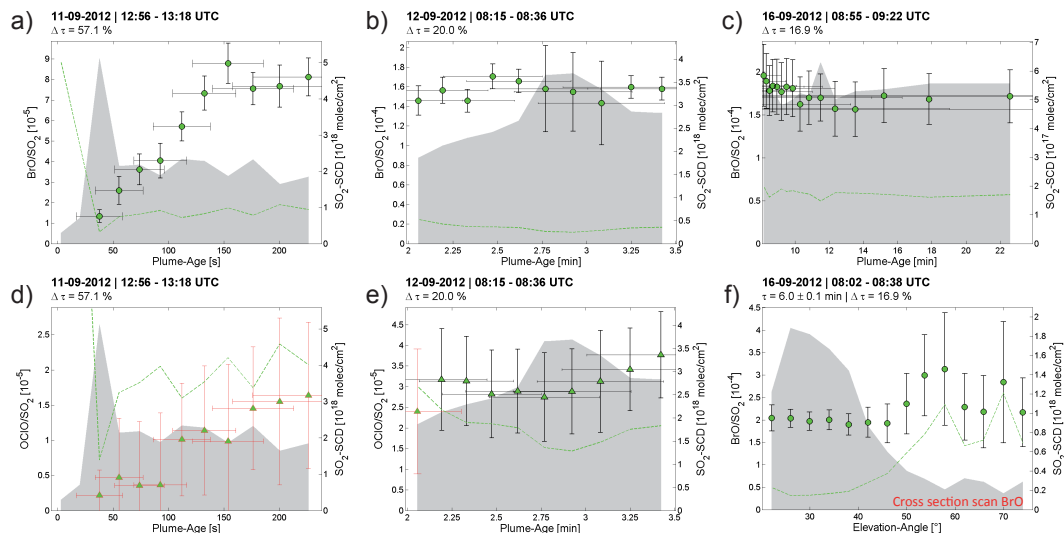
Figure 8. Plume evolution scans (see Fig. 2) of $OClO/SO_2$ and BrO/SO_2 **(a–e)** and a sample cross section scan of BrO/SO_2 **(f)**. The BrO/SO_2 ratio (green circles) and the $OClO/SO_2$-ratio (green triangles) are plotted with their corresponding detection limits (green dotted line). Red error bars indicate measurements below the respective detection limit. The SO_2-SCDs are plotted as grey shaded areas (right axis). We observed increasing BrO/SO_2 and $OClO/SO_2$-ratios in the young plume ($\tau \lesssim 3\,\text{min}$, **a, d**) and a levelling off at larger plume ages **(b, e)**. Note that in **(d)** the $OClO/SO_2$-ratios are technically below the detection limit. Nonetheless, relative trends of the $OClO/SO_2$-ratio are still reliable (for details see Sect. 3.1.1). For plume ages between 8 and 22 min **(c)** we found a rather stable BrO/SO_2 ratio with indications of a slight decreasing trend between eight and ten minutes downwind. This is probably due to a superimposed vertical profile (for details see text). In **(f)**, a cross section scan of BrO is plotted. The scan was performed directly before **(c)** and at a plume age of $\tau = 6\,\text{min}$. The BrO/SO_2-ratio increases at the edge of the plume by 30 % from 2.0×10^{-4} (plume centre) to 2.6×10^{-4} (see also Sect. 3.1.2).

Title Page

Abstract | Introduction

Conclusions | References

Tables | Figures

|◀ | ▶|

◀ | ▶

Back | Close

Full Screen / Esc

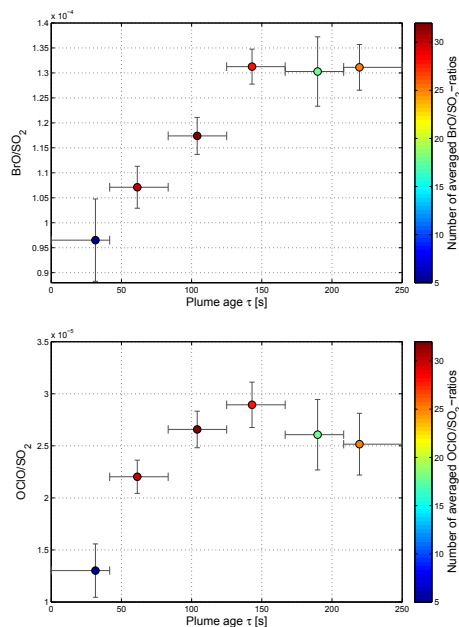Printer-friendly Version

Interactive Discussion

Figure 9. The young plume evolution of the BrO/SO_2-ratio (top) and the $OClO/SO_2$-ratio (bottom): the colour code indicates the number of averaged individual measurements. The errors of the ratios were determined from the uncertainties of the individual measurements using gaussian error propagation (for details see text). The horizontal errors denote the respective plume age interval, which was used for averaging. The position of the averaged ratios for each plume age interval represents the mean plume age of the individual spectra included in this range. For both species, we observed an increase in the young plume levelling off at $\tau = 142$ s. For larger plume ages, the BrO/SO_2-ratio stays rather constant (at $\sim 1.3 \times 10^{-4}$) whereas the $OClO/SO_2$-ratio slightly decreases.

Full Screen / Esc

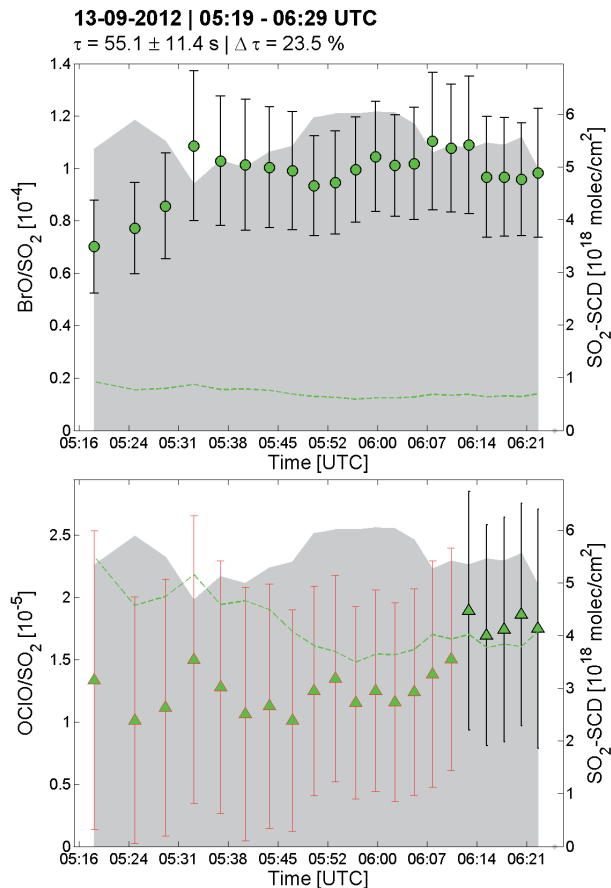Printer-friendly Version

Interactive Discussion

Figure 10. Early morning point measurement of BrO and OClO: the BrO/SO$_2$-ratio increases between 05:17 and 05:32 UTC (top). The corresponding OClO/SO$_2$-ratio also shows indications of an increase levelling off approximately 40 min after BrO (06:13 UTC).
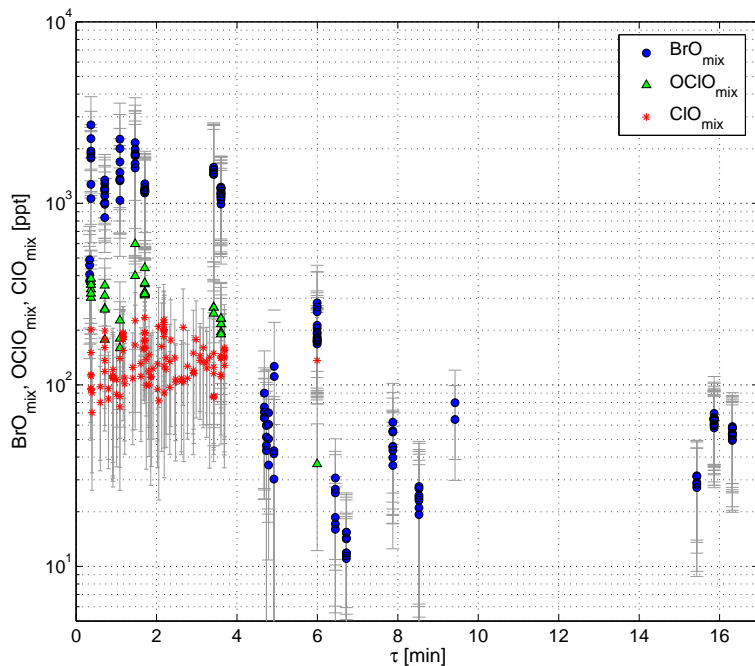
Title Page

Abstract | Introduction

Conclusions | References

Tables | Figures

|◄ | ►|

◄ | ►

Back | Close

Full Screen / Esc

Figure 11. Mixing ratios for BrO and OClO as a function of the plume age τ. The mixing ratios of BrO and OClO were determined from the respective SCDs by estimating the effective length of the absorption light paths for each spectrum (see Sect. 2.5). The ClO mixing ratios were determined from the BrO and OClO-SCDs assuming equilibrium between the formation and destruction of OClO (Sect. 2.6). The retrieved values are between 70–235 ppt (ClO), 373–2700 ppt (BrO) and 159–597 ppt (OClO) in the young plume (i.e. $\tau < 4$ min) with mean abundances of $\overline{ClO} = 139$ ppt, $\overline{BrO} = 1.35$ ppb and $\overline{OClO} = 300$ ppt. Due to plume dispersion, the concentrations decrease with increasing plume age as is indicated by the BrO results.

Title Page

Abstract · Introduction

Conclusions · References

Tables · Figures

|◄ · ►|

◄ · ►

Back · Close

Full Screen / Esc

Printer-friendly Version

Interactive Discussion

OClO and BrO observations in the volcanic plume of Mt. Etna
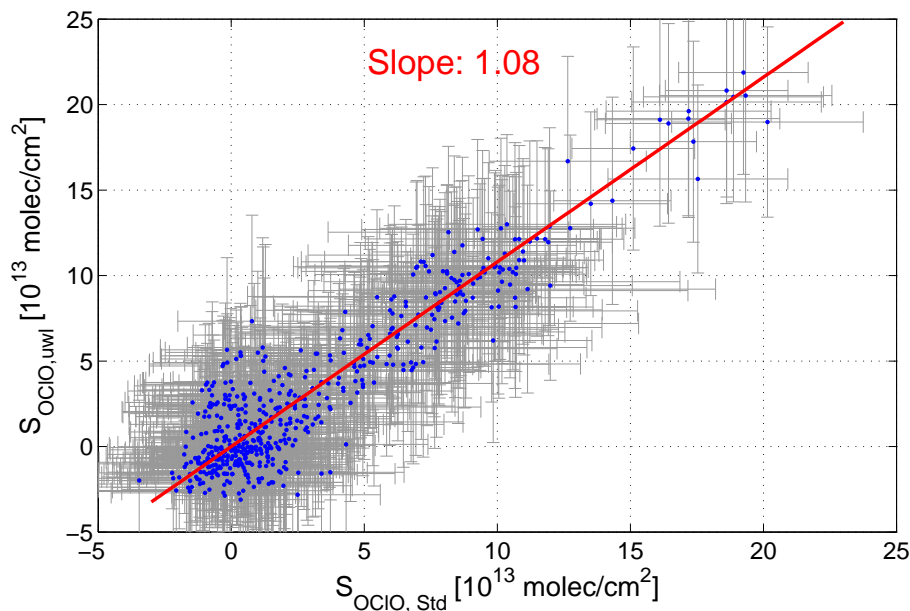
Gliß et al.

Figure A1. Retrieved OClO-SCDs from the standard evaluation range OClO$_{std}$: (330.6–356.3) nm and the second evaluation range OClO$_{uwl}$: (363.6–391.3). A mean deviation of approximately 8 % between both ranges was found with higher values in the upper wavelength range.
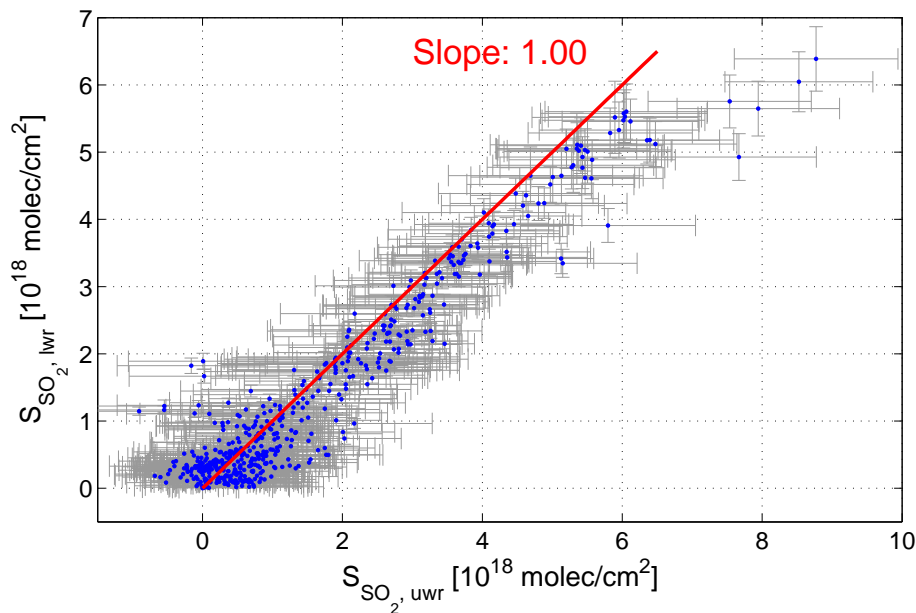
Figure A2. Retrieved SO_2-SCDs from the two SO_2 evaluation ranges. The evaluation scheme centred around 360 nm ($SO_{2,uwr}$) is plotted on the x axis, the scheme centred around 320 nm ($SO_{2,lwr}$) on the y axis. The red line indicates perfect correlation between both ranges. In case of large SO_2-SCDs (i.e. $S_{SO_2} > 3 \times 10^{18}$ molecules cm^{-2}), the retrieved SCDs in the lwr-range are more and more underestimated. For smaller SCDs, a good correlation is observable with an increased scattering in the uwr-range at low SCDs (due to the small SO_2-absorption cross section in this range, for details see Sect. 2.4.4).